UNIVERSITÀ DEGLI STUDI DI PADOVA

DIPARTIMENTO DI BIOLOGIA

Corso di Laurea magistrale in Molecular Biology

TESI DI LAUREA

Pharmacological modulation of the Wnt/β-catenin signaling rescues pathological signatures of Arrhythmogenic Cardiomyopathy in desmoplakin-deficient zebrafish models.

Relatore: Prof.ssa Natascia Tiso
Dipartimento di Biologia

Correlatore: Dott. Giovanni Risato
Dipartimento di Scienze Cardio-Toraco-Vascolari e Sanità Pubblica

Laureando: Samuele Ravarotto

ANNO ACCADEMICO 2021/2022

TABLE OF CONTENTS

ABSTRACT

Arrhythmogenic Cardiomyopathy (AC) is an inherited heart disorder characterized by the progressive fibro-fatty substitution of the ventricular myocardium, which jeopardizes the transmission of the contraction signal and increases the risk of a sudden cardiac death, particularly in young adults and athletes. About 50% of AC cases are determined by mutations in genes encoding for desmosomal proteins, including desmoplakin (DSP), whose mutation characterizes our zebrafish models.

In this thesis we aimed to characterize stable *dsp* knock-out (KO) zebrafish lines to identify early pathological features, at rest and under physical effort, and test the efficacy of pathway-directed drugs.

At larval stage, mutant larvae presented cardiac-specific abnormalities associated with developmental delay, bradycardia and alteration of the Wnt/β-catenin pathway – a key modulator of AC pathogenesis.

A series of pharmacological treatments with SB216763, an agonist of the Wnt/β-catenin pathway, rescued pathway activity, bradycardia phenotype and cardiac-specific alterations. At adult stage, histological analysis of mutant zebrafish hearts revealed an abnormal ventricular shape, with vessels dilation and adipocytes infiltration, and a general worsening of the pathological phenotype after physical training.

To conclude, our work depicts zebrafish as a suitable system to recapitulate, study and treat AC through the modulation of Wnt/β-catenin signaling.

1. INTRODUCTION

1.1. *Arrhythmogenic Cardiomyopathy*

Arrhythmogenic Cardiomyopathy (AC) is one of the leading causes of sudden deaths in young adults and athletes (Thiene *et al.*, 1988; Basso *et al.*, 2009). This disease is known as a predominantly dominant inherited heart pathology whose main phenotypical signature is the progressive substitution of the cardiac myocytes – mostly in the right ventricle (RV) – with fibrous and adipose tissues (Thiene *et al.*, 1988, Corrado *et al.*, 2017). The progressive loss of ventricular myocardial tissue causes the isolation of the healthy cardiomiocytes within the fibro-adipose matrix, which leads to the impairment of the contraction signals transmission, and is thus responsible (among other factors) for the insurgence of myocardial atrophy, aneurysms, syncopes, palpitations, and ventricular arrhythmias; leading, in the worst case scenario, to a lethal heart's stroke.

Initially, the disease was thought to affect only the right ventricle, and hence referred to as Arrhythmogenic Right Ventricular Cardiomyopathy (ARVC) (Thiene *et al.*, 1988). Later, after the discovery of others forms, affecting either the left ventricle or both (bi-ventricular forms), the name was changed to the more general Arrhythmogenic Cardiomyopathy, summarizing all the possible phenotypic expressions of the disease (Sen-Chowdhry *et al.*, 2008; Corrado *et al.*, 2017).

AC-related fatalities are strictly associated with the difficulties that its prompt diagnosis implies. AC is in fact a heterogeneous disease, both clinically and genetically, whose features can vary from almost (if not totally) asymptomatic (especially in the first phases) to severe, and its main pathological signatures – presence of fat cells inside the myocardium and the ventricular wall thinning – are frequently over-relied as the only diagnostic factors in the MRI (magnetic resonance imaging) analysis, thus increasing the rate of misdiagnosis which can result to be fatal (Bomma *et al.*, 2004).

The complexity of diagnosis itself (consisting on a scrupulous multifactorial analysis – histological, genetical, ECG - electrocardiogram - shape interpretation) and the genetic background of the AC, which can manifest itself either in a dominant – most of the times – or recessive way, depending on the type of

mutation and the gene affected, are others potential factors of error (Corrado *et al.*, 2017).

To further complicate the situation, as found out by Akdis in 2017, the hormonal context of the individual is also important, justifying the male-related-susceptibility (sex ratio 3:1) that characterizes this kind of pathology (Akdis *et al.*, 2017).

For all these reasons (and for the *sudden cardiac deaths* – SCD – that characterize most of the undiagnosed cases) AC's prevalence in the population oscillates approximately between 1:2000 and 1:5000, with the latter frequency considered as the most reliable (Basso *et al.*, 2009; Corrado *et al.*, 2017).

Italy – and Veneto region in particular – represents one of the most affected areas, where AC-related SDCs among young adults are estimated to be significantly higher respect to the worldwide ones (20% vs 10 - 15%) (Corrado *et al.*, 2017). As correctly suggested in the Corrado's study, though, this discrepancy in the incidence estimation does not allows us to consider AC as a Venetian (or Italian) specific disease, since the scrupulous, systematic investigation of SCD cases that characterizes these particular geographical regions can somehow alter the perception of AC as a worldwide equally distributed pathology (Corrado *et al.*, 2017). Founder genetic mutations have in fact been found throughout Europe and America.

1.1.2. Pathogenesis of Arrhythmogenic Cardiomyopathy.

AC's progression can be summarized into four different stages.

A concealed-initial phase, where no structural changes (or very subtle changes) can be distinguished in the right ventricle's region – increasing the rate of misdiagnosis.

A second phase, in which the first episodes of ventricular arrhythmias, palpitations and syncopes start to be associated with overt structural changes and abnormalities in the RV (wall thinning and atrophy).

A third phase, characterized by a contraction impairment of the RV, leading to the chamber failure.

A final, bilateral stage, leading to a complete loss of the pump functional stability due to the critical episodes of ventricular fibrillation (VF) and tachycardia (VT) (Corrado *et al.*, 2017). Noteworthy is the fact that a SCD fatality, despite being more frequent in the last, more severe phases, can occur at any time, even in the

first-asymptomatic stages, justifying, more than other AC-related fatalities, the definition of *sudden* (without a clue) that we all know of.

As aforementioned, AC's pathogenesis is strictly related with the progression of its main phenotypical signature: the fibro-fatty substitution of cardiac myocytes.

This particular feature – that specifically distinguishes AC from other types of cardiomyopathies (*e.g.* dilated cardiomyopathy) – depends upon the differentiation of a specific type of progenitor cells, called *fibroadypocyte progenitor cells* (FAP), capable, as the name suggests, to become either fibrocytes or adipocytes (fat cells).

The FAPs differentiation is the result of a complex molecular signaling that is triggered by the structural destabilization of the cardiac muscle. The process is thought to initially start in the epicardium (the external, protective layer of the heart) and consequently progress to eventually become transmural (*i.e.* affecting the whole myocardium), isolating muscles cells and jeopardizing the transmission of the contraction signal (Basso *et al.*, 2009) (Corrado *et al.*, 2017). An interesting point is that the fibro-fatty substitution appears to happen in specific anatomical districts of the right ventricle myocardium (the inferior, the apical, and the infundibular walls), identifying the so called "triangle of dysplasia" (see Figure 1.1.); a hallmark of AC disease that can be also used as an important diagnostic factor (Basso *et al.*, 2009) (Corrado *et al.*, 2017).

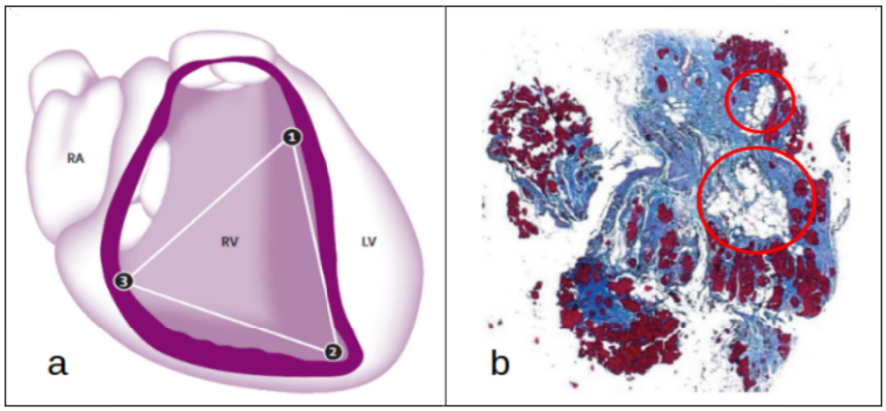

Figure 1.1. ***Arrhythmogenic Cardiomyopathy pathological signatures.*** a) Schematic representation of the right ventricle triangle of dysplasia. b) Histological endomyocardial section with abundant fibrous-fatty replacement (blue staining identifies connective-fibrous tissues surrounding adipocytes islands – in the circles). From *Arrhythmogenic right ventricular cardiomyopathy.* Basso *et al.*, 2009. The Lancet.

Another fundamental, critical aspect of AC's pathogenesis is the acceleration and worsening of its phenotypical signatures – dimension/number of the fibrous-fatty scars and thinning of the ventricles' walls – in the presence of an intense type of training (Basso *et al.*, 2009) (Corrado *et al.*, 2017).
To understand this point, which is also the reason why AC specifically affects – more than other categories – young-adults and athletes, we have to focus on the genetic nature and background of the disease, describing its implications in the molecular interplay which, most of all, triggers the fibro-fatty substitution.

1.1.3. *Genetics of Arrhythmogenic Cardiomyopathy.*

Arrhythmogenic Cardiomyopathy is commonly described as a cell-to-cell junction cardiomyopathy (Calore *et al.*, 2015; Corrado *et al.*, 2017). In fact, most of the cases are linked to mutations in junctional complexes of the intercalated disc (ID) – the anatomical structure that functionally connects adjacent cardiac myocytes. Such complexes are, by definition, the *fascia adherens,* the gap junctions and the desmosomes.
Desmosomes, in particular, generally known as the mechanical junctions of the eukaryotic cells (see below), play a crucial role on AC's onset, accounting for more than 50 % of the cases due to the causative-mutations that affects all of their major structural components (see Table 1.1.) (Giuliodori *et al.*, 2018) (Calore *et al.*, 2015) (Corrado *et al.*, 2017).
The structural destabilization of the desmosomal complexes is, at the same time, responsible for the instability of the cardiac muscle and for the molecular mechanisms that triggers the fibro-fatty substitutions (Corrado *et al.*, 2017).

Gene	**Protein**	**Location**
JUP	Plakoglobin	Desmosome
DSP	Desmoplakin	Desmosome
PKP-2	Plakophilin-2	Desmosome
DSG-2	Desmoglein-2	Desmosome
DSC-2	Desmocollin-2	Desmosome
TMEM43	Transmembrane protein 43	Nuclear envelope
LMNA	Lamin A-C	Nuclear envelope

Gene	Protein	Location
DES	Desmin	Intermediate filaments
CTNNA3	Alpha-T catenin	Area composita
PLN	Phospholamban	SERCA
TTN	Titin	Sarcomere
SC5NA	Sodium V-gated channel	Plasma membrane
CDH2	Cadherin-C	Area composita
TGFB3	Transforming growth factor	Extracellular

Table 1.1. List of the 14 genes linked with AC. From *Arrhythmogenic Cardiomyopathy.* Corrado *et al.* Circulation Research 2017.

For those reasons, in case of an intensive physical activity, which drastically increase the heart rate, the already destabilized desmosomal complexes are subjected to an even stronger disruptive force, thus increasing the detachment of neighbouring myocardial cells, the replacement with non-conductive fibro-fatty scars and the probability of a SCD related fatality. Among all the structural components of the desmosomal complex, desmoplakin (DSP), the most abundant one, represents one of the key factors in AC, being responsible, *per se*, of 10-15% of the AC desmosomal-mutations (Pilichou *et al.*, 2016). Furthermore, AC8, the autosomal dominant desmoplakin-dependent AC form (Rampazzo *et al.*, 2002), is considered one of the most challenging from the clinical point of view, being less identifiable due to its left-dominant manifestations (Giuliodori *et al.*, 2018). Despite its clinical peculiarity, though, this variant is not independent from the molecular cascade of events which underlies, as a common denominator, all AC forms, connecting the junctional dysregulation to the fibro-fatty substitution. This mechanism, which also relies on the dysregulation of one the major developmental signal, the Wnt/β-catenin pathway, will be discussed later in the introduction (Lorenzon *et al.*, 2017) (Yuan *et al.*, 2021).

1.1.4. Treatments.

AC therapies are inevitably connected with a prompt diagnosis, which, nowadays, remains the most important element for the SCD prevention.

This aspect underlies the critical importance of the genetic screening of the individuals: 1) whose relatives experienced SCD, 2) that had episodes of arrhythmia and/or other related heart's dysfunctions during everyday life and – most importantly – during an agonistic type of activity (Corrado *et al.*, 2017). In fact, a mutation in one of the genes listed in Table 1.1. is sufficient to classify that person as a potential AC "case".
The specificity, and efficacy, of the diagnosis (and of the screening itself) can be further improved by a parallel *post-mortem* histological analysis of the SCD related cases, identifying the pathological hallmarks that characterize AC onset and progression.

Once the disease (or its premature signatures) has been diagnosed, the spectrum of the potential therapeutical approaches varies, depending on the AC's stage and severity, from mild-conservatory strategies, aiming to change the lifestyle of the patient (*e.g.* avoidance of highly demanding physical activities in case of a desmosomal mutation) to more drastic, technical solutions, such as the implantation of an ICD – implantable defibrillator – device or, in the worst case scenario, to a heart transplantation.
Some pharmacological treatments are also suitable: β-blockers (which decrease the heart's rate through the competition with the epinephrine signal) and anti-arrhythmic compounds are the most common type of drugs, usually combined with lifestyle changes in the so called AAD (Anti Arrhythmic drugs) therapy (Basso *et al.*, 2009) (Corrado *et al.*, 2017).

As we understand, all these kinds of strategies do not really focus on what is the genetic and molecular nature of the pathology, only indirectly limiting – through their palliative effect – the detrimental effect of its progression.
For this reason, the research is nowadays focused on the discovery of new drugs, potentially targeting (and preventing) the molecular mechanisms which constitute the backbone of the disease.
A significant example, in this sense, is represented by the Asimaki's study. In 2014 this research team discovered a molecule, SB216763, that, by modulating the Wnt signaling, is able to recover the electrophisiological alterations of cardiac cells in two different desmoplakin-deficient animal models: zebrafish (*Danio rerio*) and mouse (*Mus musculus*) (Asimaki *et al.*, 2014).

This aspect introduces the aim of our work, which highlights the importance of zebrafish as a model for AC, and of the SB216763 drug as a new, potential pharmacological treatment.
The role, effect and efficacy of the SB216763 drug will be discussed later as well.

1.2. *Desmosomes*.

Desmosomes are the mechanical junctions of the eukaryotic cell, connecting adjacent cells in those tissues/organs (such as skin, heart and bladder) that face a high level of mechanical-associated stimuli, like friction, tension and contraction.
Their capability to confer resistance to such level of strong and continuous mechanical stresses is based on their tight association with the intermediate filaments (IFs) of neighboring, adjacent cells, transmitting the signal to the cytoskeleton so that (by becoming a functional unit) they respond to it – the mechanical stimulus – in a uniform, non-disruptive way.
These protein complexes, in their functional definition, are always considered in combination with the IFs (whose composition varies depending on the tissue), forming the so called DIFC (Desmosome intermediate filaments complexes), whose intricate structure can be subdivided into three different layers (Garrod & Chidgey, 2008); an extracellular/intercellular part, responsible for the adhesion with the other half of the desmosomal complex (thus, with the adjacent cell) and two other intracellular sections, whose main role is to associate with the IFs and transfer to them the mechanical stimulus (see Figure 1.2).
As demonstrated by several disease-inducing mutations, each of these three layers is fundamental for the mechanical-stress response, given that, being their proteins so tightly associated with each other (functionally and structurally), the disruption of any of them can result in the failure of the entire complex (Garrod & Chidgey, 2008).
Nonetheless, the extracellular portion – formed by homophilic and heterophilic interactions between the desmosomal cadherins (calcium-dependent adherins) desmoglein and desmocollin – considered its crucial location, can be viewed as the main player of the desmosomal dynamics, being capable, when necessary (*e,g.* in epidermal wound healing) to modify the strength (and adhesiveness) of the cell-to-cell contact, switching the desmosome state from a calcium-independent highly adhesive state to a calcium-dependent "weak" adhesion state (or vice-versa) (Garrod & Chidgey, 2008).

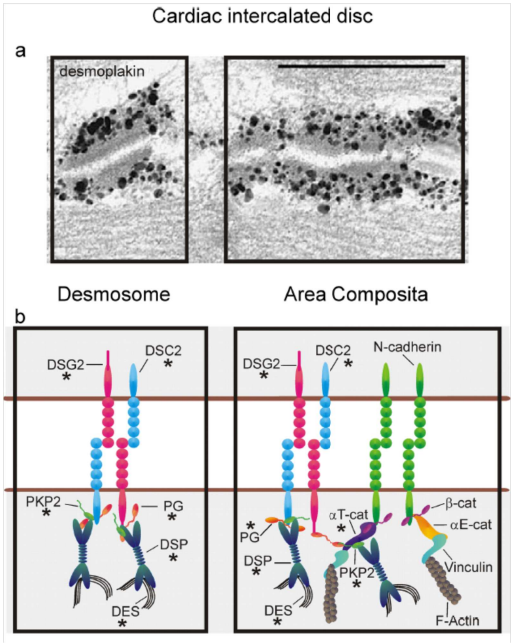

Figure 1.2. ***The desmosomal complex.*** a) TEM (Transmission electron microscope) immuno-electro micrographs showing desmoplakin location within the intercalated disc. b) Desmosomal architecture: structure and domains. From *Arrhythmogenic cardiomyopathy: a disease of intercalated discs*. Springer. Calore *et al.*, 2014.

The switch between these two mutually exclusive states is triggered by an internal signaling, modulating the activity of the protein kinase C (PKC), the Ca^{2+} concentration and, consequently, the activity of the two desmosomal cadherins, which, in the highly adhesive state, assume a highly organized-packed conformation.

Beside their structural role, desmosomes are also involved in the signaling transduction, mostly by regulating/changing the availability of signaling-related proteins; plakoglobin, that together with desmoplakin represents one of the leading AC-factors, but also the extracellular cadherins desmoglein and desmocollin, which are known regulator of cell proliferation, differentiation and tissues' morphogenesis (Garred & Chidgey, 2008).

Additionally, we have to consider the indirect effect – on these kinds of signaling – of the other demsosomal proteins (*e.g.* desmoplakin), which, being fundamental for the stability of the complex, can impact and modify the pool of those signaling proteins. Focusing on the heart, then, desmosomes, being, as already mentioned, located in the intercalated discs with the gap junctions, which electrically connects

adjacent cells, are directly implicated in the transmission of the contraction signal. The disruption of the tissue's integrity induced by their structural instability is affecting the progression of the electrical stimulus which is responsible for the uniform and synchronous contraction that characterizes heart's dynamics. In other words, the disruption of the functional unit – normally granted by the electrical and mechanical linkage between adjacent myocytes – is interrupting the normal, proper communication between the cells, thus provoking the arrhythmia episodes which are symptoms – beside AC – of a heart malfunctioning (Delmar & McKenna., 2010). This phenomenon, the desmosomal contribution to the arrhythmia insurgence, is further enhanced by the fibro-fatty substitution.

In fact, a part from its mechanical/physical implications in the contraction impairment, desmosomes' instability – as previously announced – is promoting the activation of the molecular cascade which leads to the myocytes's replacement. Despite the progress in identifying the genes responsible for AC, though, the mechanism by which alterations in desmosomes trig this phenomenon is still not well understood. The mechanism is thought to depends upon the release of plakoglobin, which, by interfering with the Wnt signal, is able to regulate (indirectly) fibrogenesis and adipogenesis related genes (Basso *et al.*, 2009) (Lorenzon *et al.*, 2017) (Yuan *et al.*, 2021).

Anyway, recent studies on genetically modified cellular and animal models showed a connection between mutation in junctional/desmosomal proteins and the dysregulation of other important signaling pathways, such as: TGFβ and Hippo/ YAP-TAZ pathways, suggesting a possible interplay (connection) between the Wnt dysregulation and these two other signaling pathways (Garcia-Gras *et al.*, 2006) (Lorenzon *et al.*, 2017) (Giuliodori *et al.*, 2018).

We thus understand why desmosomes, just like any other kind of protein complex, having multiple roles and associated functions, are so pivotal in several kinds of diseases, among which AC (Garrod & Chidgey, 2008) (Delmar & McKenna., 2010).

1.2.1. Desmosomal architecture: proteins and domains.

Extracellular portion. It is mainly composed by the two desmosomal cadherins, desmocollin and desmoglein, which span the plasma membrane (PM) and interact with their own counterparts (homophilic and heterophilic interactions) in the

intercellular space, forming a ladder of dimers through an N-terminal β-strand interaction of their E1 domains.

Desmocollin (DSC). In humans, it has 3 different isoforms (DSC 1, 2, 3) and its structure is composed by an intracellular anchor (IA) domain, used to bind the intracellular desmosomal plaque (described below), a transmembrane (TM) domain, with which it associates with the bilayer of phospholipids, and – at the N terminus – four different EC (Extracellular cadherin repeats) sites, whit the first one, EC1, also named CAR domain, that is responsible for the heterophilic interaction with the DSGs in the neighboring cell.

Desmoglein (DSG). It has 4 different isoforms (DSG 1, 2, 3, 4), and its structure is almost identical to the DSC's one, with just one relevant difference in the C-terminus, where a domain called RUD – composed by a variable number of 29 amino acids (AAs) (amino acids) repeats and whose function is still unknown – contains some strong PKC phosphorilation sites.
Furthermore, as members of the cadherins family, these proteins have Ca^{2+} binding sites interspersed between the extracellular domains; fundamental, as the name *cadherin* suggests, for the proper binding and functioning (rigidity) of the protein.

Intracellular portion. Two main structural domains compose the intracellular portion of the desmosomal complex. An outer dense plaque (ODP), composed by the Armadillo (*arm*-repeats domain) proteins plakoglobin (JUP) and plakophilin (PK), and an inner dense plaque (IDP), resulting from the desmoplakin-IFs interaction.

Plakoglobin (JUP): Its main structural feature is the presence of a central Armadillo domain, consisting – in JUP case – of 12 *arm* repeats (42 AAs units) which are responsible (as a known protein-protein interaction domain) for the binding: 1) of the desmosomal cadherins and 2) of the N-terminus of desmoplakin, allowing the creation of the proteins-chain which connect the extracellular portion of the desmosome to the IFs. Plakoglobin is mostly linked with recessive forms of AC and its mutation has been found in only 1% of the cases (Lorenzon *et al.*, 2017); despite its minor contribution to the pathology, though, plakoglobin resulted fundamental for its initial description, seen the homozygous JUP mutation that characterizes the Naxos disease – an inherited

cardiocutaneous disorder which is comprehensive of AC and of a peculiar epidermal phenotype, with woolly hair and palmoplantar keratoderma (Corrado *et al.*, 2017).

Plakophilin (PKP): It has 3 different isoforms (PKP 1, 2, 3), distinguished by their tissue-specific expression and their subtle structural modifications. All of them possess 9 *arm*-repeats in the central domain, plus a flexible loop (between repeats 5 and 6) which is responsible for their curved structure. As JUP, PKP's main role is to act as a structural factor, binding to several partners (among which the IFs) to confer a higher stability to the overall complex. Of particular interest is the PKP2 isoform, which is, by far, the desmosomal gene mostly linked with AC onset, with a frequency of mutation that ranges from 10% to 45% of the cases (Lorenzon *et al.*, 2017).

1.2.2. Desmoplakin.

Desmoplakin (DSP) is the most abundant protein of the desmosomal complex, acting – via its association with the other structural components – as a molecular bridge, connecting IFs elements (in case of the myocytes, desmin) to the plasma membrane (Yuan *et al*., 2021).
DSP, as the key factor for desmosomal stability, finds its major expression in epithelial cells (mostly skin cells), conferring, with its structural partners, the mechanical-stress resilience that guarantees the integrity of the tissues.
Its mutations, thus, causing the unstableness of the whole desmosomal complex, are associated with a series of life-threatening pathologies, which vary, in their detrimental effect, according to the level of DSP functional impairment (*e.g.* neonatal death – *lethal acantholytic epidermolysis bullosa* – in case of a C-terminal domain loss) (Garrod & Chidgey, 2018). Being DSP fundamental for the proper myocardial development, most of these pathologies affect heart's stability and function.
Apart from AC (AC8 in particular), other kinds of cardiomyopathies, and strictly related diseases, are associated with a *DSP* gene mutation. That is the case, for example, of the dilated cardiomyopathy (DCM) – characterized by the heart's chambers dilation – and the Carvajal syndrome, another rare autosomal recessive form of AC (Corrado *et al.*, 2017).

Beside its structural role, fundamental for heart's stability, desmoplakin is also involved – in combination with other cellular players – in other clinical features of AC's pathological context, among which: inflammation, cell conductivity reduction and adipogenesis (Yuan *et al*., 2021).
Its down-regulation has in fact been linked, in cultured cells, with a decreased level (and abnormal distribution) of $Na_v1.5$ channels, negatively impacting the total Na^+ current, slowing the conductivity pace and thus – in an *in-vivo* context – increasing the number of arrhythmic episodes.
DSP involvement in inflammation and adipogenesis is instead dependent on the specific activation of cellular mediators, NF-kB (nuclear factor kappa B) and *neurofibromin-2* (NF2) respectively, which, triggered by the DSP mutation, turn on their signaling pathways (NF-kB and Hippo) and lead, eventually, to the establishment of those pathological signatures (recruitment of macrophages, increased inflammatory cytokines expression and adipogenic-apoptotic episodes enhancement) (Yuan *et al*., 2021).
Lastly, Desmoplakin mutation, as discussed, is also impacting the Wnt/βcat signaling, which, being pivotal for AC pathogenesis (Lorenzon *et al*., 2017) (Calore *et al*., 2015), is underlining, once again, the critical importance of this protein for AC onset and progression.

1.2.2.1. DSP structural features.

DSP structure, just like any other member of the plakin family, is tripartite, with two globular domains (at the N and C terminus) separated by an α-helical coiled-coil rod region (Yuan *et al*., 2021). This central rod domain is thought to be necessary for the protein dimerization, while the N-terminal domain (also called plakin domain), consisting in two pairs of spectrin repeats (three antiparallel helixes) separated by a Src-homology-3 (SH3) domain, is used for heterophilic protein-protein interactions, connecting desmoplakin with the ODP components. The C-terminus, in the same way, is composed by three plakin repeats domains PRDs (named A, B, C), with the latter two, B and C, that, given their grooved globular shape, are considered the putative IFs binding sites (Garrod & Chidgey, 2008).
C-terminus, whose ablation is lethal, is also important for the DSP regulation, containing, at its extreme end, a glycine-serine-arginine rich site whose phosphorylation is modifying the DSP-IFs binding affinity.

Human desmoplakin exists in three different isoforms (DSP I, DSP Ia and DSP II), which vary in their length (rod domain composition) and are produced by an alternative splicing of the DSP gene (chromosome 6p24.3) (Yuan *et al*., 2021) (Figure 1.3).

The longest isoform, DSP I, is predominant in the myocardium, while the intermediate (DSP Ia) and the shortest (DSP II) ones are mainly expressed in other anatomical regions (aorta and skin, respectively). Nonetheless, DSP II mRNA has been recently found in the left ventricle (LV) and atrium (LA) as well, adding new insights (and complexity) to the complete dissection of DSP role in the AC pathological context (Yuan *et al*., 2021).

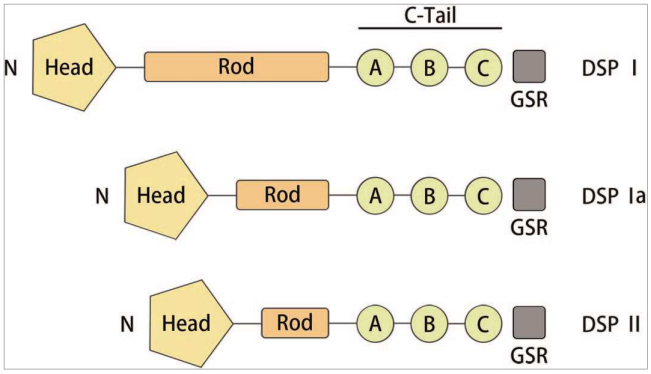

Figure 1.3. ***Desmoplakin isoforms and structure***. From: *Desmoplakin and clinical manifestations of desmoplakin Cardiomyopathy*. Yuan et al., Chinese Medical Journal - 2021.

1.3. The Wnt pathway.

The Wnt pathway, known as one of the major developmental signals, is a highly conserved paracrine, cell to cell signaling cascade which – given its crucial importance – is implied in a wide variety of cellular processes, acting from the embryonic stage (in which, for instance, it is responsible for the A-P – anterior posterior – axis induction and specification) to the adult stage, where it promotes – among other effects – tissues' homeostasis and renewal (Lorenzon *et al*., 2017).

Such broad spectrum of action is, most of all, referable to its well-known capability to influence (and control) cells' proliferation, differentiation and fate; a feature that – with the signal dysfunction – is connected with a series of

developmental and hereditary problems, such as obesity and cancer (MacDonald *et al*., 2009).

The Wnt signal, considered in its general description, comprehends a bunch of different types of pathways, distinguished – in their function – by their specific signaling molecules (Wnt ligands) and intracellular mediators (*e.g.* β-catenin, calcium and PKC - protein kinase C).

The canonical pathway, which is a key factor for our discussion on AC, relies on β-catenin transduction, and, as the term "canonical" suggests, it represents the paradigm – and foundation – of all the other Wnt signals. For that reason, it is universally referred as the most important and common one.

1.3.1 Signaling cascade description (canonical pathway).

As for any other kind of cellular signaling, the Wnt pathway has an ON and an OFF state, depending on the presence (or absence) of the ligand triggering the intracellular cascade.

In the OFF state, determined by the absence of the ligand, the intracellular transducer, β-catenin, is phosphorylated by the so-called destruction/degradation complex; a cytosolic unit that is responsible, due to the synergistic action of its components (APC, Axin, GSK3 and CK1), for the control of β-catenin's activity.

In particular, the post-translational phosphorylation of β-catenin (AA residues - Ser33, Ser37, Thr41 and Ser45) carried out by the enzymatic components of the destruction complex (GSK-3 and CK1 - casein kinase 1), triggers its ubiquitination (β-Trcp E3-ligase) and consequent destruction in the proteasome.

The suppression of β-catenin's migration into the nucleus is, as a consequence, causing the inhibition of gene expression, with the nuclear factor, *groucho* – the negative regulator of the Wnt signal –, that binds to the TCF/LEF transcriptional complex and interferes with the genes expression (Lorenzon *et al*., 2017) (MacDonald *et al*., 2009).

Conversely, in the ON state, the Wnt ligand (a cysteine-rich glycoprotein), secreted by the neighboring cells, binds to the frizzled (Fzd) receptor and the LRP 5-6 co-receptors in the plasma membrane and triggers the recruitment of a new player - dishevelled (Dvl) - to the intracellular portion of Fzd.

Dishevelled, being capable of sequestering some components of the destruction complex (GSK3 and Axin) to the PM, releases β-catenin action, allowing its migration into the nucleus and the consequent activation of the Wnt-responsive

genes (among which c-myc, cyclin D1, and the auto-regulative - negative effector - *Axin-2*). This general mechanism varies – at different levels – according to the typology of the Wnt ligand (19 different isoforms discovered in humans), the frizzled receptor (10 isoforms) and the intracellular transducers, thus highlighting the complexity (with all the possible signaling combinations) that characterize this pathway.

1.3.2. Wnt signaling in the heart.

Being one of the major developmental signals, the Wnt pathway plays a crucial role in organs' formation and morphogenesis. Focusing on the heart, its premature suppression has been linked with malformations in different anatomical districts, such as the outflow tract, the valves and the endocardial layers (Lorenzon *et al.*, 2017).
Furthermore, being the Wnt signaling responsible for cell differentiation and fate, it represents a key factor for the maintenance of the spatial heterogeneity – in terms of cell types – that characterizes the normal mammalian cardiac environment (composed by myocytes, fibrocytes, smooth muscle cells, endothelial and epicardial cells).
In particular, a complex interplay between the canonical and non-canonical Wnt pathways is responsible for the maintenance of this equilibrium, with the canonical pathway that is mostly implied in the regeneration and homeostasis of the tissue, keeping the precursors of the cardiac cells in a proliferative-active state, while the non-canonical (β-catenin independent) cascades are – on the other hand – mostly involved in all the differentiation phenomena (Lorenzon *et al.*, 2017).

1.3.3. Wnt pathway and AC.

Despite being not fully understood, in its pathological contribution, the Wnt pathway, well-recognized as the key regulator of the cardiac homeostasis, plays a pivotal role in AC's study (Rampazzo *et al.*, 2014) (Calore *et al.*, 2015) (Lorenzon *et al.*, 2017) (Yuan *et al.*, 2021).
As mentioned in the previous paragraphs, its possible interplay with other signaling pathways – *i.e.* Hippo/YAP-TAZ and TGF-β pathways – is thought to be

at the basis of the adipogenesis and fibrogenesis phenomena, connecting the desmosomal instability to the change in genes expression.

In particular, the dysregulation of its activation state (ON - OFF), together with the simultaneous activation of the Hippo and TGF-β signals, appears to be fundamental for the insurgence of these pathological signatures (see Figure 1.4.).

Regarding the adipogenesis, the canonical Wnt signal, impacted by the destabilization of the desmosomal complex – and/or of the adherens junctions in the IDs –, seems to be down-regulated (if not completely suppressed) by a mechanism that relies both on plakoglobin release and Hippo pathway's activation.

In particular, the simultaneous activation of the Hippo signal, caused, in the same way, by the ID's instability (which leads to the expression of neurofibromin-2 (*NF2*) gene – a known trigger of Hippo signaling), is sequestering, through its intracellular mediator YAP (Yes associated protein) β-catenin in the cytosolic compartment, impeding its migration into the nucleus and – hence – the consequent transduction of the canonical signal, with an increase in the expression of differentiation (adipogenesis-inducing) genes (Lorenzon *et al*., 2017).

Conversely, in the fibrogenesis, the Wnt activation state seems to be unchanged, with the TGF-β (SMADs) signaling that, being activated by a JUP disruption on some experimental models (Li *et al*., 2011), replaces the Hippo pathway in the interplay phenomenon with the canonical Wnt signal.

On the other hand, though, as a counter-proof of the necessity of the signaling interplay for the expression of all the main AC signatures, the activation (and up-regulation) of the canonical Wnt signal – due to the AKT (protein kinase B) activation and GSK3 suppression – appears to be the only factor required for the hypertrophy/dilation of the right-ventricle myocytes that characterizes the acute, final phases of the AC (Corrado *et al.*, 2017) with the over-expression of cell-cycle/proliferative related genes (e.g cyclins and c-myc) and a consequent dilation of the ventricle (Li *et al.*, 2011) (Lorenzon *et al.*, 2017).

These examples, each differently supported by experimental data (Lorezon *et al*. 2017), are highlighting, once again, all the difficulties and controversies (different activation states, signaling interplay) that characterizes the canonical Wnt signal, thus suggesting its intricate and thus not fully comprehended role in AC's onset and progression.

Despite these debates, though, the general "idea" about AC's pathogenesis is that the down-regulation (and suppression) of the canonical Wnt pathway determined by plakoglobin release into the nucleus (conversely to what suggested by another

study, with a cardiac JUP deletion in a mouse model) (Li J. *et al.*, 2011) is fundamental for the pathology's onset and progression (Calore *et al.*, 2019) (Giuliodori *et al.*, 2018) (Garcia-Gras *et al.*, 2006) (Yuan *et al.*, 2021). Plakoglobin, in fact, belongs to the same protein family of β-catenin, the catenins family, and when released into the cytosol (*i.e.* as a consequence of the desmsosomal destabilization) is able to compete with it for the TCF/LCF transcriptional complex, to promote its degradation and to affect, thus, the progression of the canonical Wnt signal (Yuan *et al.*, 2021).
Despite sharing a high percentage of identity (88%), in fact, these two catenins still have subtle changes – mostly at the level of the N terminus and C terminus – that differently impact: 1) their capability to form a working ternary complex with the DNA, and, 2) their opposite role in the transcription of Wnt-responsive genes (Zhurinsky *et al.*, 2000) (Garcia-Gras *et al.*, 2006) (Yuan *et al.*, 2021).

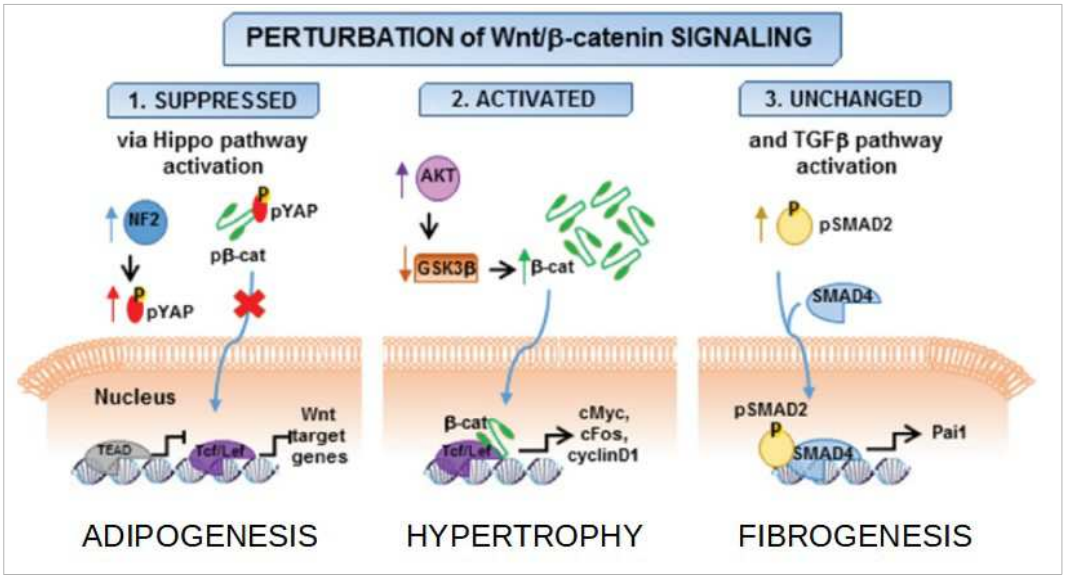

Figure 1.4. ***Wnt/β-catenin pathway in AC.*** Signaling involvement and interplay in the AC's pathological context.
From *Wnt/β-catenin pathway in Arrhythmogenic Cardiomyopathy.* Oncotarget. Lorenzon *et al.*, 2017.

As Corrado and collegues suggested, the suppression of the canonical Wnt signaling determined by plakoglobin release is – as a response – increasing the level of non-canonical signaling proteins (such as Wnt5b and BMP7), which, in

turn, stimulate the differentiation of the FAP cells into myocardial adipocytes (Corrado *et al*., 2017).
At the same time, the Hippo signaling, activated, as well, by mutations in the desmosomal complex, is helping the differentiation of the FAP cells by reinforcing the down-regulation of the Wnt signal (see Figure 1.4.)
As we will see, this "general" model is consistent with our findings on a desmoplakin deficient zebrafish (Danio rerio) line, further supporting the down-regulation of the Wnt signal as a common-crucial event for AC's pathogenesis.

1.4. The zebrafish model organism.

The model organism *Danio rerio*, zebrafish, is a small, freshwater fish – family of *Cyprinidae*, class of *Actinopterygii* (bony fishes) – naturally distributed in tropical areas.
Its common name, zebrafish, derives from the characteristic presence of some horizontal blue stripes that run all along its body, and, although other mutant types of liveries (e.g leopard *Danio rerio*) are present, this specific "zebra" phenotype, constituting the "default", wild-type (WT) livery pattern, justifies the usage of the general denomination "zebrafish" (Figure 1.5).
Just like any other model organism, *D. rerio* has a series of advantages (technical as well as functional) that contributed to its spread in the biological research; becoming, in a short time, one of the most recent (yet used) animals in the field.
First of all, due to its small dimensions (average body length 4-5 cm) it can be easily maintained and bred, with the constitution of appropriate facilities and enclosure areas. Secondly, its high fertility rate (about 200 eggs per coupling) and rapid development (sexual maturity in ≈ 3 months), allow the collection of a significant amount of data, whose statistical reliability, due to the increased number of samples, is definitely more solid than that obtained from mammalian model organisms (e.g. mice).
Focusing more specifically on the technical advantages for the biological research, one of the major benefits of *D. rerio*'s usage is the optical transparency that characterizes its embryonic and larva stages; a feature that, among other advantages (e.g.: tracking a florescent signal), allows a real-time, *in vivo* analysis of several developmental defects and diseases (Lieschke & Currie, 2007). Also, being its genome highly similar to the human's one (more than 80% of the human genes have an orthologous counterpart in *Danio rerio*), its genetic manipulation –

facilitated by the availability of forward and reverse genetic approaches, such as CRISPR/Cas9 technique – permits the creation of mutant and reporter transgenic lines (fluorescent reporter lines) that can be used to model a specific disease or pathological condition.

From this point of view, the zebrafish, due to its rapid development, high fertility and optical transparency, is the ideal model organism for drug discovery and treatment (Lieschke & Currie, 2007) (Asimaki *et al*., 2014).

On the other hand, one of its main disadvantages (compared to other model organisms) is the partial genetic duplication that – being zebrafish a teleost fish – characterizes its genome; a features that, with two potential genes for a given human counterpart, increases the amount of work and the necessity of interpretation.

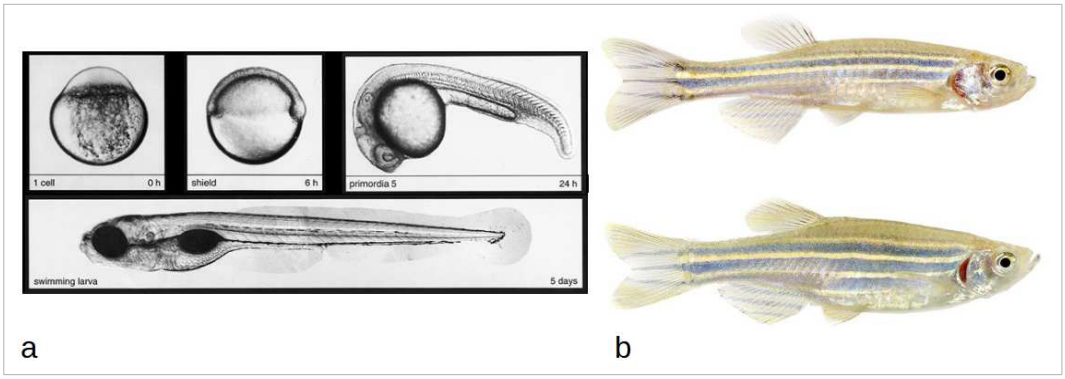

Figure 1.5. ***Zebrafish developmental stages*****.** a) embryonic and larval stages (1 cell stage – 0 hpf, shield stage – 6 hpf, primordia 5 embryo – 24 hpf, swimming larva – 5dpf). b) adult male (top) and female (bottom) zebrafish.
Sources:http://zebrafishlab.be/media-gallery/detail/8/22https://chandrasekhar.biology.missouri.edu/stages-jpg-2/

1.4.1. Zebrafish as a model for AC study.

As we have just discussed, the zebrafish model organism, despite being, as obvious, less similar to humans – in terms of functional and anatomical features – than its mammalian counterparts (i.e. mouse), still has some important advantages that allows its exploitation as a disease model for a wide variety of human pathologies.

Focusing on heart-related diseases, and, more specifically, on AC itself, these advantages become so useful that *D. rerio* can be wisely considered one of the main choices for this kind of studies.

First of all, its heart, even if different from the human's one, with only two chambers (an atrium and a ventricle), an outflow tract and an afferent *sinus venosus* (see Figure 1.6), is perfectly mimicking, in its shape and motion (contraction), the functionality of the mammalian organ. Secondly, being its rate (WT ≈ 80 - 100 beats per minute) closer to the human's one respect to the mouse model (WT: more than 300 beats per minute), it can be exploited to study the impact (in terms of alteration of the contraction signal) given by a specific AC-inducing mutation.

This feature, combined with the optical transparency of zebrafish larvae, allows the detection, under the stereo-microscope, of arrhythmia and bradycardia episodes, whose insurgence rate, timing and worsening can thus be compared between different pools of fishes (WT and mutants) with a high reliability and statistical significance.

In addition, the availability of fluorescent-reporter lines, which can further improve this optical analysis (with the detection of structural malformations caused by the desmosomal disruption), can be exploited to study – and hopefully dissect – the complex and still debated role of different signaling pathways (Wnt, Hippo, etc.) in the AC's pathological context.

Another important advantage of zebrafish application in AC is the fact that the penetrance of this pathology (in our case the AC8 form) is, more or less, similar between human and zebrafish; this means that we can observe mutant fishes with no overt/visible phenotype (wild-type like), a mild-phenotype, or, in the last case scenario, a severe phenotype.

Eventually, the possibility to perform an intensive training – with methodologies that we will describe in the next section – both on larvae and adult fishes, allows us to study the progression and worsening of the AC in a context that, with the due differences, resembles the condition (physical exercise) to which DSP-deficient athletes are subjected. On the other hand, though, the high regeneration rate characterizing the zebrafish model could, unfortunately, impact the possibility of analysing the fibrogenesis phenomenon in an *in vivo* or histological sample, thus representing one of the main disadvantages of the zebrafish application in AC.

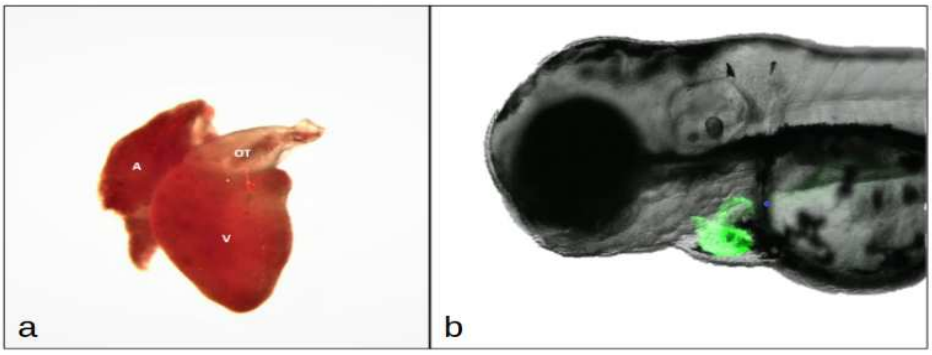

Figure 1.6. ***The zebrafish heart: adult and larval stage.*** a) Zebrafish heart (from WT adult fish) representation, with the sponge-like atrium (A), the ventricle (V) and the outflow tract (OT). b) "*Green heart*" larva (WT) imaged by merging bright-field/fluorescence microscopy.

1.4.2. Desmoplakin in Zebrafish.

As previously mentioned, the zebrafish genome is partially duplicated, having, for a given fraction of the human genes, two independent genomic loci.
In the case of the *DSP* locus, the zebrafish counterparts are represented by the *dspa* (desmoplakin A) and the *dspb* (desmoplakin B) genes, located on chromosome 2 and chromosome 20, respectively (ZFIN database - zfin.org), whose significant – yet not complete – resemblance with the *DSP* human ortholog (45-50% average similarity - http://www.ensembl.org/Homo_sapiens/Gene/Compara_Ortholog) makes them suitable for AC analysis in the zebrafish model.
As found out by Giuliodori and colleagues, both of these genes are in fact expressed in tissues affected by AC pathogenesis (*i.e:*. myocardium), and their silencing (leading to the so-called "pale-desmsomes" phenotype) is affecting the number and organization of the desmosomal complexes, whose symmetrical structure, being so drastically affected, is no longer detectable under the TEM microscope (see Figure 1.7) (Giuliodori *et al*., 2018).
As expected, *dsp* gene(s) deficiency is impacting the Wnt pathway as well (Figure 1.7), activating the Hippo signal and leading, as a result, to a developmental delay and to a series of cardiac problems (*e.g.:* heart's rate reduction) (Giuliodori *et al*., 2018).
These results, consistent with our findings, a part from reinforcing the "general idea" about the Wnt dysregulation (down-regulation) in AC, are also justifying the

choice of the zebrafish Dsp orthologues as a starting point for Arrhythmogenic Cardiomyopathy's comprehension and study.

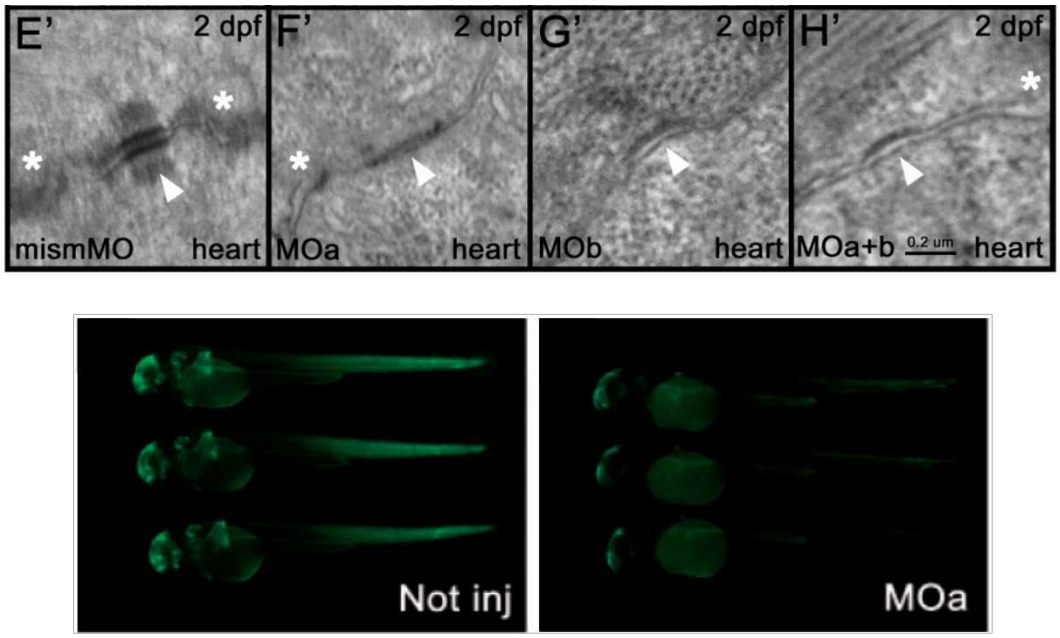

Figure 1.7. ***Desmoplakin in the zebrafish model.*** Top images: TEM analysis of cardiac samples. Morpholino-induced knock-down (silencing) of *dspa* and *dspb* causes the fading of the desmosomal structure ("pale-desmosome" phenotype; white arrows), compared to the control (mismatch morpholino) condition (E'). Bottom images: Wnt pathway (green signals) reduction in *dspa*-deficient larvae. Not injected control (left) and Morpholino-mediated *dspa* knock-down (right). From: *Loss of cardiac Wnt/β-catenin signaling in Desmoplakin-deficient AC8 zebrafish models is rescuable by genetic and pharmacological intervention*. Cardiovascular Research, Giuliodori et al., 2018.

2. MATERIALS AND METHODS

2.1. Zebrafish lines maintenance

All experiments were carried out on fishes currently available at the Zebrafish Center (Facility) of the Vallisneri building – University of Padua. The animals – separated based on their age (adult, juvenile, larvae) and genotype – were kept in a temperature-controlled environment (28.5 °C) with a 12 hrs - 12 hrs dark-light cycle, according to their circadian rhythm in the natural environment.

Zebrafish embryos were maintained in Petri dishes until 7 dpf (7 days post fertilization), manually – then automatically – fed with dry food starting from day 5 and constantly monitored throughout their permanence in the facility's nursery, with water flux control and weekly cleaning of tanks and filters.
The pairing of adult individuals (from 3 months old) was performed in specific tanks with double bottom that allows the separation of the animals from the newly-produced eggs – an essential precaution due to the natural egg-eating behavior of *Danio rerio*.
The eggs, collected with the help of a strainer, were kept in Petri dishes, cleaned (removal of unfertilized-rotten ones) and put at the optimal temperature (27-28.5) until 7 dpf.
The anesthesia or euthanesia of zebrafish embryos was performed with Tricaine (MS222; E10521, Sigma–Aldrich, Milan, Italy), a chemical compound able to inhibit the skeletal muscle activity by blocking the entrance of sodium ions and – thus – the progression of action potentials (0.16 mg/mL for anesthesia or 0.3 mg/mL for euthanasia).
Regarding adult fishes, the euthanasia methods (always preceded by the anesthetization) varied according to our purposes (*e.g.* heart extraction or whole body histological analysis).
Focusing more specifically on the genotypes, different zebrafish lines were used for our experiments. Wild type lines (Giotto and Tubingen strains), *dsp*-mutant lines (*dspa* and *dspb* lines), whose creation will be now discussed, and transgenic-reporter lines for the detection of signaling pathways expression and alteration.

In particular, two transgenic reporter lines were used in our studies:

- Wnt/ β-catenin reporter line *Tg(7xTCF-Xla.Siam:EGFP)*, which express the engineered green florescent protein (EGFP) under the control of the Wnt-responsive TCF transcriptional complex (Moro *et al.*, 2013).

- Green heart line *Tg(tg:EGFP-myl7:EGFP)*^{ia300} in which the GFP is - specifically expressed in the myocardium of the zebrafish heart (under the myosin-7 promoter) (Facchinello *et al.*, 2017).

2.2. dspa and dspb lines.

The *dspa* line was bought from the ZMP project (Zebrafish Mutation Project), as a result of the ENU (N-ethyl-N-nitrosourea) mutagenesis – a chemical forward genetic approach that randomly introduces point mutations (which are subsequently screened and isolated) throughout the genome. In our case, the *dspa* allele contained a C->T substitution on the exon 19, introducing a non-sense (premature stop codon) mutation which resulted in a C-terminally truncated protein.
Conversely, the *dspb* mutant line was created by CRISPR-Cas9 technique, with the sgRNA (single-guide RNA) targeting the third exon. The PCR screening of the F_0 generation identified, as expected, several types of mutations in the *dspb* gene, and the isolation of the germinal ones was obtained by crossing the F_0 individuals with wild-types fishes. Eventually, after the PCR genotyping of the F_1 embryos, a *frame-shift* deletion of 13 bases (*dspb* Δ13pb) was selected as the ideal one, being detectable – due to its dimensions – by a classic agarose gel electrophoresis.

2.3. Genotyping of dspa and dspb mutant lines

DNA extraction

Emrbyos at 24-48 hpf (hours-post fertilization) were placed in 0.5-mL tubes with a anesthetizing concentration of Tricaine - 0.16 mg per mL of *fish water* (0.5 mM NaH2PO4 ; 0.5 mM Na2PO4 ; 1.5 g Instant ocean salts ; 2 mg/L Methylene blue) for 2 minutes. After that, the solution was discarded, replaced with 50 µL of the DNA lysis buffer (NaOH 50 µM) and the samples were heated at 85-90 °C for 20 minutes in a thermoblock.
At the end of the heating procedure, the tubes were put at 4°C for 5 more minutes, and 5 µL of TrisHCl 1 M pH 7.5 were added.
The DNA extraction of adult fishes was performed with a similar procedure. A small piece of the caudal fin was cut, inserted into 0.5-mL tubes with 50 µl of the lysis buffer (NaOH 50 µM) and heated for 20-25 minutes in the thermoblock. After that, the samples – containing the DNA in solution – were ready for PCR amplification and genotyping.

Genotyping

Characterization of *dspa* and *dspb* loci in mutant fishes were performed independently - according to the different nature of the two mutations. Since the *dspa* line bears a point mutation (substitution), not modyfying the allele length, compared to the wild-type locus, the sequencing of the PCR product was required. Conversely, the *dspb* line, bearing a 13 bp deletion, was identifiable with a classic electrophoresis in a 3.5 % (w/v) agarose - TBE (Tris Borate EDTA) buffer gel.
The following PCR primers were used in the process:

Gene name	Forward primer (5'-3')	Reverse primer (5'-3')	Product size (bp)
dspa	ATCGAGGAGGAAAAGCGCAA	GCCTCATCCTGCAGCTGTAA	194
dspb	CAAAATGGGCCCGGATGAG	AGCTTCTGGTCTTCGGCTC	114

Table 2.1. DNA primers for *dspa* and *dspb* mutant line genotyping.

2.4. Heart rate estimate at larval stage (3 - 5 - 7 dpf).

Zebrafish larvae were anesthetized in Petri dishes with Tricaine (1 mL in 25 mL of fish water) and placed under the dissecting microscope (Leica M165FC) for subsequent analysis. Heart beats were visually counted – with a single-larva magnification – in 15 seconds time intervals. Each heart was checked three times (15 seconds each), and the average result was then multiplied by four, in order to obtain the beats per minute (bpm) statistics.

2.5. Morphological analysis.

Wild type and desmoplakin-deficient embryos (3 dpf) were anesthetized, placed in Petri dishes (or microscope slides) with 2% methyl-cellulose and consequently oriented (lateral view) under the dissecting microscope (Leica M165FC).
Bright field images were acquired with a Leica DFC7000T camera at 3x - 10x magnification, focusing on the entire embryo and the cardiac region, respectively.

Morphological alterations in the cardiac region, such as dilation, edemas and blood effusion, were compared between the two pools (as % on the total embryos), statistically analyzed and graphed with GraphPad Prism 7.04.
ImageJ software was used to measure cardiac region's dimensions and dilation, with embryos' total length and eye-size (generally recognized as developmental indicators) as normalizing factors.
Morphological comparison of hearts was also performed, extracting the organ from adult fishes (1 year old) – with tweezers and other dissection instruments – and subsequently acquiring them with the same aforementioned instrumental settings.

2.6. RNA isolation and real-time PCR (qRT-PCR)

Samples (larvae or extracted adult hearts) were initially homogenized with glass beads in a *tissue-lyser* machine (Tissue Lyser II - QIAGEN) for 3 minutes at the maximal speed. Total RNA was separated with the TRIzol - chloroform method (500 and 100 µL, respectively), precipitated with 250 µL of isopropanol and subsequently quantified and checked – for DNA / protein contamination – at the NanoDrop (Thermo Scientific, Milan, Italy) instrument (260/280 260/230 ratios).
For gene expression analysis, 1 µg of purified RNA was retro-transcribed – according to samples' concentration – with random primers and the M-MLV Reverse Transcriptase RNase H - (Solis BioDyne, 06-21-010000). Real-time quantitative PCR (qPCR) was performed in triplicate (10 µl per well) with the ×5 HOT FIREPolEvaGreen qPCR Mix Plus (Solis BioDyne, Tartu, Estonia) and Light Cycler 480 II (Roche, Monza, Italy).

Gene name	Signalling pathway	Forward primer (5'-3')	Reverse primer (3'-5')	Product size (bp)
gapdh	Housekeeping	GTGGAGTCTACTGGTGTCTTC	GTGCAGGAGGCATTGCTTACA	173
ccnd1	Wnt/β-catenin	CCAACTTCCTCTCGCAAGTC	TGGTCTCTGTGGAGATGTGC	123
myc	Wnt/β-catenin	AGAAAGCTGGAGTCCTCGAC	CTGCTGCAGTGTGTTCAGC	118

Table 2.2. Real-time primer sequences for gene expression analysis.

Canonical Wnt signaling dysregulation was tested with primers for β-catenin-responsive genes (*c-myc* and cyclin D1), and the housekeeping gene *gapdh* – coding for the glyceraldehyde-3-phosphate dehydrogenase – was used as a positive control.

2.7. Immunofluorescence analysis.

Embryos at 3 dpf were initially fixed in 4% paraformaldehyde (PFA) O/N at 4°C and stored at -20°C in methanol (MeOH) 100%.
In the first part of the procedure, the samples were progressively rehydrated with a series of 5-minute MeOH/PBS washes (75% MeOH 25% PBS, 50% MeOH 50% PBS, 25% MeOH 75% PBS), depigmented with a 2% H_2O_2 + 3 % KOH bleaching solution and eventually permeabilized – to allow the entrance of the antibodies – by a 7-minute freezing step at -20°C in acetone.
At the end of the permeabilization step, embryos were washed with distilled water, then in 1X PBS + 0.5% Triton and subsequently blocked for 30 minutes with a PBDT (PBS 1X + 1% DMSO + 1% BSA + 0.5% Triton X) + 2% goat (or sheep) serum solution, to saturate non-specific binding sites.
To test the cardiac region inflammation, the samples were then incubated for 2 days at 4°C with primary antibodies targeting the L-plastin protein (a leukocyte-expressed protein) in a 1:5000 concentration (1 µL of antibodies in 5 mL of PBDT + goat serum).
Unbound primary antibodies were removed with four washes in PBDT (15 minutes x wash), and secondary alkaline phosphatase (AP) conjugated antibodies were subsequently incubated, in a 1:1000 concentration, overnight at 4°C.
As previously, excess of solution was washed in PBDT and the fast-blue - naphthol staining was eventually performed. This type of staining relies on the hydrolytic nature of the AP enzyme, which removes phosphate groups from the naphthol AS-MX substrate and produces a colored (blue) precipitate after the coupling between the newly produced phenolic compound and the fast blue salts. The fast blue staining allows to detect a signal both in the bright field – where the colored precipitate can be used to check the efficacy of antibodies incubation – and in the fluorescent spectrum, which the emission of a far-red signal that identifies, specifically, the localization of the protein of interest.
After the removal of the staining solution, the samples – now ready for the acquisition – were then either conserved in the dark at 4°C in PBS 1X or directly mounted on glass slides with glycerol.

Fast blue fluorescent signal was detected at the confocal microscope (Leica TCS SPE), and Z-stack images of the cardiac region were subsequently analyzed with the ImageJ software.

2.8. Histological analysis.

Euthanized adult zebrafish (from 3 to 12 months old) were fixed with the Bouin solution (70% Picric acid + 25% Formalin + 5% Acetic acid) for at least 24 hrs at RT, depending on the dimension and quantity of the samples. To allow a better perfusion of the Bouin solution – by eliminating the formation of air sacks – the samples were pierced in the abdominal region and the caudal fin was also partially removed. Once fixed, the samples were washed with ethanol 70% + ammonia (NH_3) at RT until they became completely white, dehydrated with a gradual series of ethanol washes (80%, 95%, 100% EtOH) and eventually cleared with xylene 100%. Xylene treatment was arrested once the samples appeared to be completely translucent, with the brain region and the swim bladder clearly distinguishable inside the body.
After two other washes in 50 % xylene - 50 % paraffin, the samples were included in paraffin and subsequently sectioned for the hematoxylin & eosin (HE) staining that was conducted according to standard procedures.
Images of whole-body sections were eventually acquired at the Leica M165FC microscope, specifically focusing on the cardiac region.

2.9. Mortality rate assay.

To study the mortality rate, zebrafish larvae were monitored for 30 days starting from 3 dpf, counting the number of deaths for each conditions (wild-type, mutant, treated larvae) on a daily basis and eventually constructing a Kaplan-Meier curve (a classic estimator for survival / death rates) with the collected data.

2.10. Birefringence assay.

The birefringence assay exploits the optical properties of highly organized-ordered matter – such as sarcomeres structure – to rotate a polarized light according

to a specific orientation and retry, consequently, structural information on the base of that (Smith *et al.*, 2013).
In our case it was performed to asses the level of skeletal muscle myofibril alterations in 5 dpf zebrafish larvae. Anesthetized embryos were placed in 2 % methyl cellulose – as previously described – and subsequently placed on a glass slide. The specimen was then inserted between two polarizing-rotating filters and subsequently analyzed under a Leica M165FC microscope.
Skeletal muscle intensity was recorded in bright field with a DFC7000T digital camera, rotating the upper polarizing filter until the light refracted by the skeletal-muscles was uniform and homogeneous all along larvae's body. The pixel intensity was then analyzed with the ImageJ software, normalized for the samples' length due to the slight differences, in terms of size, that characterize different pools of larvae (wild type and mutant) in the first stages, and consequently analyzed with the GraphPad Prism software.

2.11. Physical training of zebrafish larvae.

To evaluate the effects of the physical training on the zebrafish larvae, pools of animals were placed either in 6-well plates or 25 mL petri dishes for 5 and 10 days respectively, with a 1 % methyl-cellulose fishwater solution to increase the viscosity of the medium. Larvae's movement was triggered with the addition of a stimulus (food) inside the medium, whose high density impacted the normal motion of the animals and thus promoted their physical training.
The procedure was repeated each day, counting the number of deads per condition. At the end of the experiment data were compared and analyzed for significant differences. Resting larvae (wild-type and mutant) were monitored for 10 days as control pools.

2.12. Physical training of adult zebrafish.

Three-month old zebrafish (mutant and wild-type) were trained for 3/6 months in a purposely constructed *swim tube,* consisting on a fish tank attached to an electrical pump which allows the generation of a strong water flux (see figure 2.1.). The water pump had three different power levels, with the third one that corresponded to a 85 cm/s output, way higher than the flux speed of zebrafish

natural environments (between 3.5 - 13.9 cm/s) (Arunachalam *et al.*, 2013). The different zebrafish pools were subjected to 1 hour of intense workout (maximal speed flow) for five days/week, allowing the mechanical stress recovery during the week-end. Resting fishes were taken as controls, and at the end of the training period histological samples of sacrificed fishes were analyzed after the hematoxylin & eosin staining.

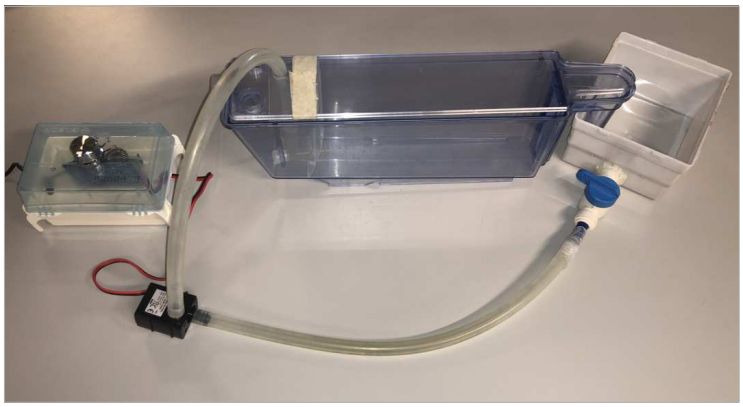

Figure 2.1. ***Swim tube representation.*** Experimental set up for the physical training of adult zebrafish.

2.13. Pharmacological modulation of the Wnt/β-catenin pathway.

Pharmacological assays were performed with two different drugs: SB216763 (SB) and XAV939 (XAV), respectively activating and inhibiting the canonical Wnt pathway. Specifically, the SB agonist destabilizes the destruction complex, inhibiting the GSK3-β activity and thus promoting the progression (and activation) of the signaling pathway (Asimaki *et al.*, 2014), while the XAV molecule stabilizes the destruction complex by inhibiting the Tankyrase (TNKS) protein, which normally promotes Axin degradation (Ma *et al.*, 2015).
Zebrafish larvae were treated for 2 days with either 40 µM of SB or 5 µM of XAV, directly dissolved in the fish water. The only exception is represented by the methyl-cellulose training experiment, in which the timing of the SB treatment has been extended, with the same concentration, throughout the analysis. The optimal concentration of the two drugs was previously assessed through a series of dose-dependent screenings.

2.14. Statistical analysis.

Graph Pad Prism V7.0 software was used for the statistical analyses. Pairwise comparisons of two samples were performed with the unpaired t-test method, while multiple comparison analysis was carried out either with the non-parametric (Kruskal-Wallis) or the parametric analysis of variance (ANOVA) tests, according to the assumption of normality. Suvival rates analyses were instead performed with the Log-Rank (Mantel -Cox) method, a non-parametric test which is commonly used for these kind of experiments. In the charts, error bars display standard errors of the mean. Asterisks indicate significant differences from controls. Correspondence between asterisks and significance levels is indicated in the figure's captions.

3. LINES CHARACTERIZATION – SELECTION OF THE AC MODEL

The project of this thesis is based on the double heterozygous mutant line (dspa +/- dspb +/-), whose pathological phenotype was previously assessed and selected as the ideal for AC's study after a series of lines' characterization experiments. These passages, that will be now briefly described, are also preparatory for the understanding of the consequent output; we report here the main results and implications.

3.1. Lines characterization.

3.1.1. *Morphological analysis.*

Desmoplakin deficient zebrafish embryos (3 dpf) were analyzed for the presence of morphological alterations in the cardiac region – such as dilation, edemas, and blood effusion – respect to the WT animals, taken as reference. The different genotypes (*dspa* -/- *dspb* +/+, *dspa* +/+ *dspb* -/-, *dspa* +/- *dspb* +/-) were compared to each other, taking the eye size and the body length – generally considered as benchmarks of the zebrafish development – as normalization factors.
In Figure 3.1. a panel with representatives examples of the different genotypes illustrates all the cardiac alterations that were considered in the analysis.

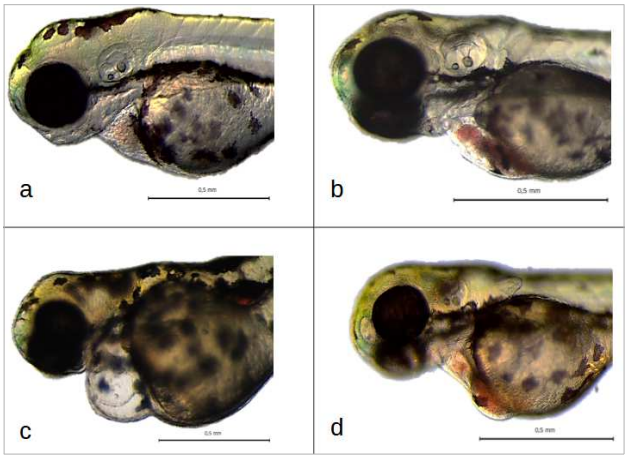

Figure 3.1.

Cardiac region morphological analysis.

a) WT ; b) dspa -/- dspb +/+ ; c) dspa +/+ dspb -/- ; d) dspa +/- dspb +/-. All samples are in lateral view. Anterior to the left.

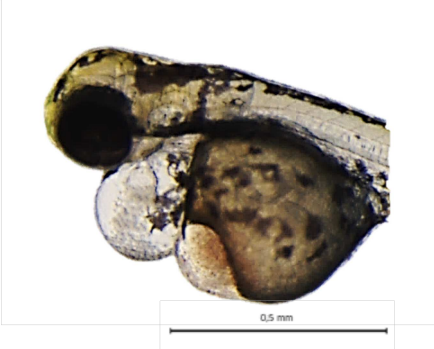

Figure 3.2. ***Double homozygous larva.*** Example of a double homozygous mutant larva presenting huge cardiac region dilation, edemas and blood effusion.

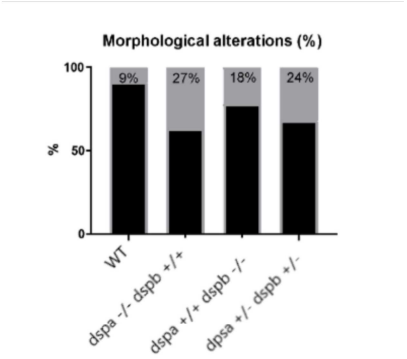

Figure 3.3. ***Quantitative representation of the morphologically altered animals.*** Graph showing the percentages of morphologically altered larvae in the different genotypes. Grey columns represent the amount of altered larvae in the considered pools.

Specifically, panel a) shows a wild-type embryo with not significant/evident cardiac alterations. Panels b) and c) show pericardial effusion and cardiac dilation examples respectively, with fluids accumulations (edemas) in both examples. Panel d, instead, represents an embryo with a phenotype that is comprehensive of all the considered alterations.

At the end of the process all the morphological alterations were counted, and the different genotypes were classified on the basis of their overall cardiac defects

(percentage of animals which presented at least one morphological signature in the considered pool) (see Figure 3.3.).

As Figure 3.3. shows, all the mutant genotypes showed a significant increase in the number of such specific defects, with a mean percentage of affected animals that was more than doubled respect to the WT pool.

In particular, the *dspa* -/- and the DH (Double Heterozygous) mutant lines displayed the worst phenotype, with a comparable amount of altered cardiac regions (27 % and 24 %, respectively) in the pool. This result exemplifies the variable effect (detrimental effect), in terms of pathological manifestations and degree of structural impairment, induced by the desmoplakin mutation, with a penetrance which is thus attested to be around 30%.

The double homozygous mutant line (*dspa* -/- *dspb* -/-), that overall was the one with the highest level of morphological alterations (see Figure 3.2.) was not considered in the final results since the structural impairments caused by the double mutation were so detrimental that the life expectancy of the mutant animals was extremely low, impeding the creation of a stable mutant line.

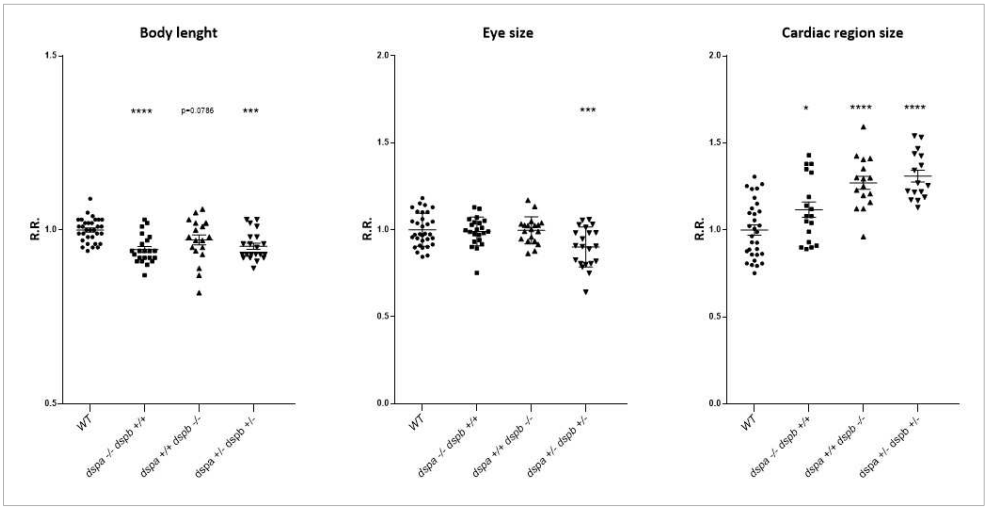

Figure 3.4. ***Body length, eye size and cardiac region area estimates.*** In the scatter plots, asterisks indicate the level(s) of significance (* p-value < 0.05, *** p-value < 0.001, **** p-value < 0.0001); R.R. is the relative ratio, indicating that each value – divided by the length of the embryo – was normalized to the WT reference pool. Sample size n = 25. Test: one way ordinary ANOVA, with α = 0.05.

The morphological characterization of the cardiac region included also the determination of its area, which was firstly normalized by the dimensions of the

considered embryo and successively compared to the WT value. This analysis, represented in Figure 3.4., is underlining, once again, the phenotypical criticality of the double heterozygous line, which showed a cardiac region size ≈ 35% higher than the WT reference.
The graph is also explaining the developmental delay which characterizes, more than the others, this DH mutant line, with a significant reduction in both body length and eye size parameters, which is accompanied, as we will demonstrate later, by a down-regulation of the Wnt developmental signal.

3.2.2 *Heart rate estimate.*

The lines characterization has then proceeded with the determination of the heart rate, tying to check for potential differences in the number of beats (per minute) of the WT and the mutant larvae. As described in the methods, the heart rate of each larva was counted three times for 15 seconds, eventually calculating the mean per minute (beats per minute) statistics. In Figure 3.5. we show the data obtained for each day of the analysis, which was repeated, identically, at different developmental stages, in order to identify possible changes in the trend of variation of this particular cardiac phenotype.

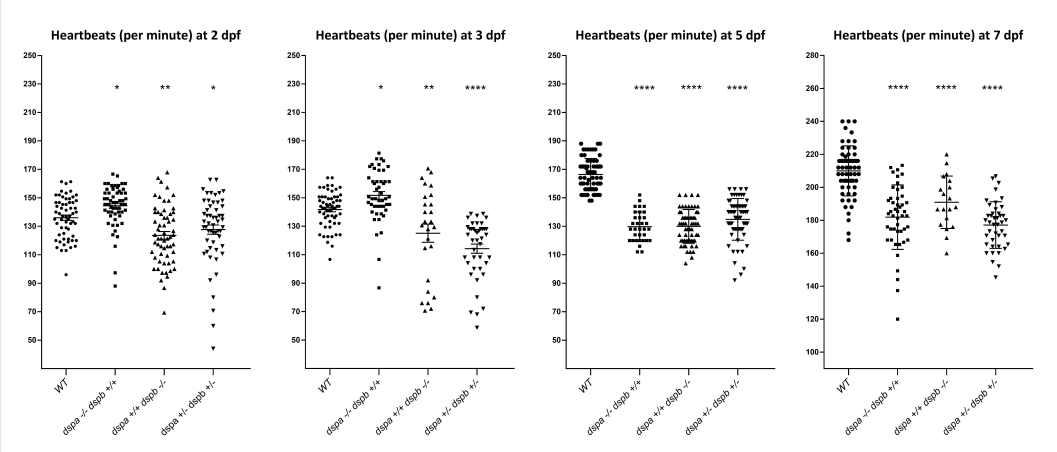

Figure 3.5. Heart rates estimates (beats per minute) for the different genotypes. Beats per minute every day of the analysis are reported and compared to the WT reference. Sample size changed in the different days: n = 50. * p-value < 0.05, ** p-value < 0.01, **** p-value < 0.0001 Test: one way ordinary ANOVA, with α = 0.05.

Looking at the scatter plots we can easily understand that all mutant lines presented a bradycardic (slowed heart rate) phenotype, which started to appear at

3 dpf and proceeded, with enhanced differences, in the following days. Also, in this case the DH line appeared to have the worst and most precocious phenotype, with a trend of bradycardia that was maintained stable throughout the analysis (four level of significance starting form 3 dpf).
In particular, the difference becomes more evident at 3 and 7 dpf, where the mean estimate of the heart beats, in the case of the DH mutant line, is reduced by approximately 20-30 beats (per minute) respect to the WT condition. This result, a part from confirming, as expected, that the structural destabilization of the desmosomal complex is impacting the transmission of the contraction signal – seen also the overall reduction that characterizes the other mutant genotypes – further suggests that the double heterozygous mutation, affecting both desmoplakin isoforms, is more detrimental than the other ones, compromising the possibility of a functional/structural compensation.
An interesting aspect of these results is represented by the 2 dpf scar plot, where we can see that the heart rate analysis is quite uninformative, with the mutant lines that presented an overall beats per minute average that was almost identical to the WT pool one.
This could be due to the fact that the differences in the heart contractions, which depend on a series of neuronal, cellular and structural communication, were still too subtle, insignificant, to be manifested at that particular age. In other words, the larvae were just too young (undeveloped) to show that kind of complex phenotype, even considering the lack of overt morphological alterations – in the cardiac region – at this particular developmental stage (2 dpf).

3.2.3. *Mortality rate estimates.*

All different pools (mutant and wild-type) were also analyzed for 30 days to assess the mortality rate of each genotypic condition. In Figure 3.6. we present the Kaplan - Meier curves resulted from this kind of analysis.
Focusing on the graph, we can immediately notice that larvae's fatalities started to occur, independently from the genotype, around 9 - 10 dpf, thus highlighting a developmental time point that can be referred to as common, critical barrier for the zebrafish larvae's survival. Secondly, we clearly observe that the curves of the different genotypes separates, starting from that point, with different slopes (pace) and amplitudes, reflecting the detrimental effects associated with each specific mutant condition. Especially, we can appreciate that around day 15 there was a

dramatic acceleration in the mortality rate of the double heterozygous pool (orange line), which again resulted to be the worst mutant condition, with a percentage of survival at 30 days that was more than three times lower than the WT pool one (17 % *vs.* 58 %).

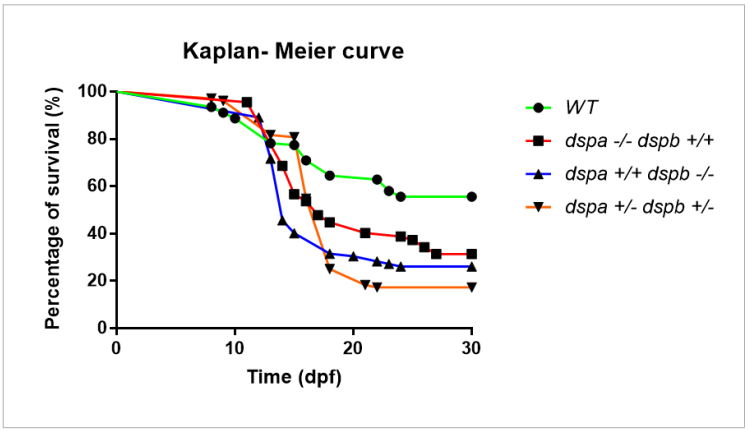

Figure 3.6. ***Survival rate analysis.*** Kaplan - Meier curves of the different genotypes represent the proportions of deaths per day. Number of samples n = 100. Test: Log-Rank (Mantel – Cox) test.

Interestingly, the DH line was, for what we have observed, the only one that experienced such sudden decrease in the survival rate, since the other mutant conditions – despite starting to die before the DH condition, around day 12-13 – continued their death trend with a constant and slower slope, eventually leading to a percentage of survival that was closer to the WT condition respect to the DH line.

This result is consistent with what was previously found for the cardiac region malformations and heart beats rates, in which the DH line showed, over all, the worst possible phenotype, further corroborating the hypothesis of an increased detrimental effect of the desmoplakin mutation when present in a double heterozygous condition.

According to this graph, then, we can also hypothesize that the turning point observed for the DH death rate (15 - 18 dpf) is indirectly highlighting the moment in which the level of damages due to the desmoplakin mutation – whose detrimental effects, as we have seen, started to be manifested since 3 dpf – reached a critical, unsustainable threshold, heavily affecting heart's function, its

stability and eventually leading, thus, to the death of the most affected/susceptible individuals.

3.2.4. *Wnt signaling pathway dysregulation (qPCR analysis)*

Real time PCR was performed on the messenger RNA transcripts (mRNAs) of two of the main β-catenin responsive genes, c-myc (*myca*) and cyclinD1 (*ccnd1*), evaluating the level of activation of the Wnt canonical signal in all different mutant conditions (see Figure 3.7.).
Looking a the scatter plots (Figure 3.7.) we can clearly see that genes' expression is significantly reduced in the desmoplakin mutant background, with a trend of down-regulation that is common, and equal in terms of significance, to all the different lines.
If we pay attention to the mean values of the Log2 FC statistics, though, we can notice that this reduction appears to be neither homogeneous nor equally strong among all the different zebrafish lines, particularly if considered separately for the two genes.
For example, we see that the *myca* mRNA appears to be reduced mostly in the *dspa* -/- and *dspb* -/- lines, while the cyclin D1 expression, on the other hand, resulted to be significantly down-regulated (p-value = 0.0154) only in the DH line.
This difference in the mRNAs production could be attributed to the peculiar and specific pattern of activation of the two genes in the Wnt canonical signal. Their expression can in fact be triggered at different time points, at different "levels" of the cascade of events that correspond to the overall molecular effects of the canonical Wnt signal, thus responding differently to specific - yet similar - genotypic conditions.
Following this kind of reasoning, we can hypothesize, hence, that the complete knock-out (KO) of one desmoplakin isoform (a condition representing the first two desmoplakin deficient lines) is affecting, differently from the DH mutation, the molecular process that leads to the c-myc expression, maybe influencing the Wnt activity by affecting the availability of the desmosomal related signaling molecules that were previously discussed.
According to this, we can see that the level of down-regulation in the *myca* expression is almost identical (same mean) in the first two mutant lines.

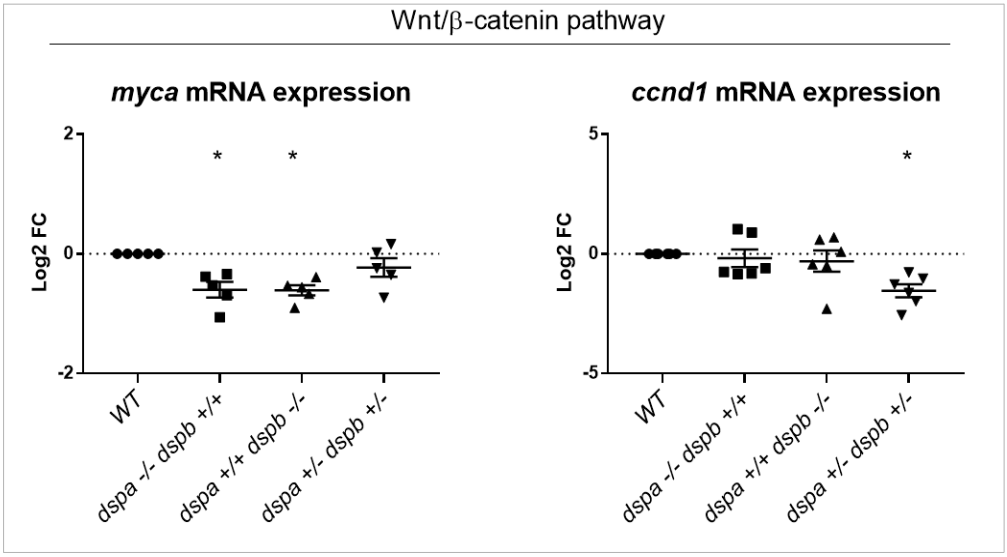

Figure 3.7. ***Gene expression analysis (qPCR) of Wnt responsive genes.***
In the y-axis, the log2FC (log Fold Change) statistics clarifies the level of mRNA changes compared to the reference (WT) control. N pools = 5, 6; embryos per pool n = 30. * p-value < 0.05. Test: non-parametric Kruskas-Wallis test, with α = 0.05.

More important, and noteworthy, is the magnitude with which the down-regulation of the Wnt signal occurs in the different mutant lines. Looking at the range of variation of the log2FC statistics, in the y-axis of the two graphs, we can see that, in fact, the *ccnd1* down-regulation is greater, in absolute terms, than *myca* one, with a final value of expression that was more than halved respect to the other gene. This aspect is suggesting that, the DH line – the only one that reduces *ccnd1* expression – is impacting, more than the other desmoplakin deficient lines, the Wnt canonical signal, provoking its down-regulation and resulting, even from this point of view, the worst mutant condition. This result takes even more significance if we consider that the qPCR analysis was conducted on the whole embryos (3dpf), not only in the cardiac region, thus the effective down-regulation that we observed in the DH line could be even greater, also justifying the absence of significance found in the case of the *myca* gene.

3.2. Selection of the double heterozygous line as the ideal AC model.

Taken together, all these results, from the morphological analysis to the characterization of the Wnt signaling dysregulation in the different mutant lines, justified our choice to focus exclusively on the DH line, selecting it as the ideal zebrafish

model for the AC study. This decision is further supported by the genetic background of this line, which better represents the dominant condition (only 1 allele mutated) that characterizes, as previously said, most of the desmoplakin-linked AC8 cases (Rampazzo *et al*., 2014). Connected to this, being both *dsp* genes expressed in the cardiac region (Giuliodori *et al.*, 2018), it seemed reasonable to work with a heterozygous model that presented a balanced dysregulation of the two proteins.

According to this, from now on, all the following results will be presented, and discussed, as a comparison between the WT and the double heterozygous condition.

4. RESULTS.

4.1. Genotyping.

Genomes of desmoplakin-deficient zebrafish lines were constantly monitored for the sake of strictness and reliability of the results.

As previously described, the characterization of the *dspb* gene was performed through PCR amplification followed by a gel electrophoresis in 3.5% (p/v) agarose (see Figure 4.1.), allowing the detection of the 13-base deletion (Δ13) that characterizes this mutant line.

According to this, looking at the gel electrophoresis example, we can easily identify the three possible genotypes. The WT reference one, in the first column, with a corresponding length of 114 bp (base pairs), the *dspb* -/- homozygous mutant, whose band is evidently lower (thus smaller) than the control, and the heterozygous *dpsb* +/- one, whose WT and Δ13 bands can be distinguished in the third and fourth columns.

The extension of the deletion can be also appreciated in the DNA sequences of the corresponding genotypes (Image 1 of Figure 4.1.), with the *dspb* -/- graph that, as expected, presented a 13-base long missing sequence in the targeted region.

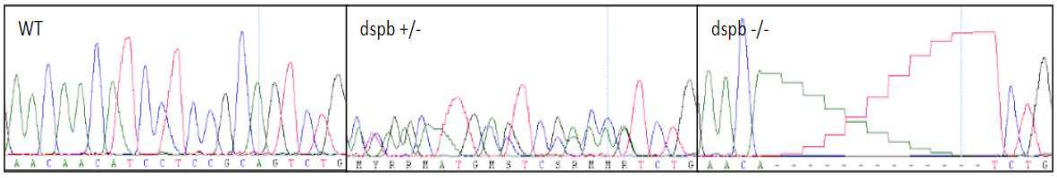

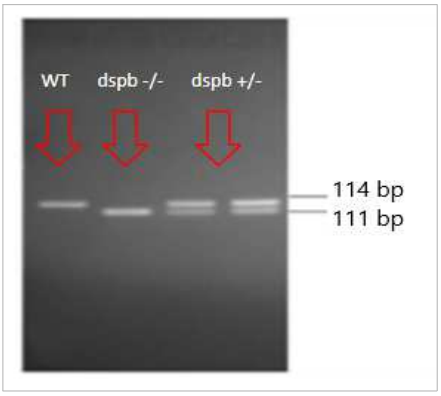

Figure 4.1. ***Genotyping of the dspb gene.*** Sequencing and gel electrophoresis of the DNA amplicons.

To identify the point mutation (substitution) of the *dspa* mutant line, the sequencing of the DNAs was necessary, having previously tested, by a 1% gel electrophoresis, the quality and efficacy of the PCR reaction. Figure 4.2 shows the sequencing results of the targeted region, where the C > T substitution can be appreciated by comparing the WT with the *dspa* -/- DNAs.

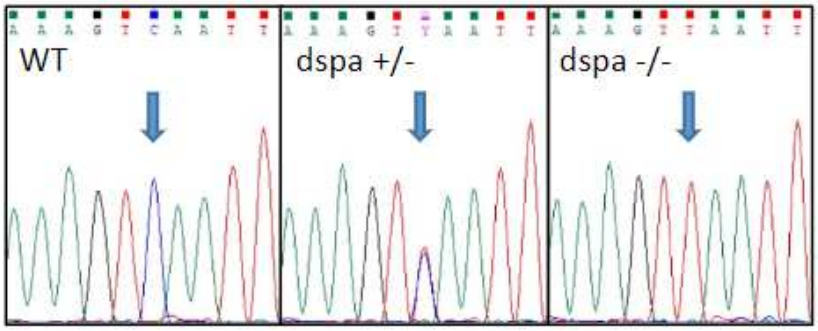

Figure 4.2. ***Sequencing of the dspa mutant line.*** Each peak represents specifically one of the four nucleotides (one color per nucleotide); the height of the peaks represents the confidence with which a given base has been called.

Specifically, as for the *dspb* graph, the first image shows a WT individual, where the cytosine (blue peak) is, as expected, unchanged. The second graph represents, instead, a heterozygous (*dspa* +/-) sample, with the two alleles that, having C or T base, produced each a corresponding peak (blue or red) with a halved height. The last example is instead representing a *dspa* -/- individual, where the blue peak of

the cytosine is absent and substituted by a red one, indicating that both alleles presented the thymine in that position.

4.2. Immunofluorescence on 3 dpf embryos.

Inflammation of the cardiac muscle has recently been described as a factor linked with AC pathogenesis (Asatryan *et al.*, 2021) (Yuan *et al.*, 2021). For this reason, we performed an immunofluorescence analysis on 3 dpf embryos pools aiming to understand whether there was a significant difference in the expression of inflammatory specific markers (L-plastin) between the WT and the double heterozygous mutants.

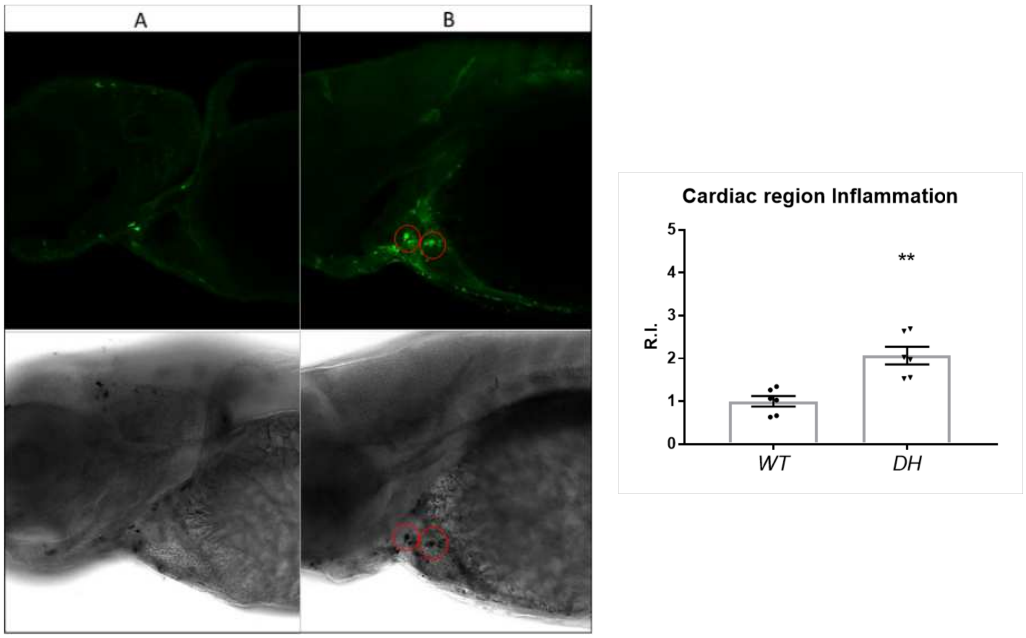

Figure 4.3. ***Immunofluorescence analysis.*** Image 1: confocal fluorescent and bright-field images of A (WT) and B (DH) embryos, compared to each other; all embryos are in lateral view, anterior to the left. Image 2: fluorescent signal quantification is graphed and reported as R.I. (relative intensity) values, subtracted to the background intensity and normalized to the WT control. Number of samples n = 6. ** p-value < 0.01. Test: unpaired t-test with α = 0.05.

In Figure 4.3., levels of fluorescence are compared between the two conditions, with an evident increase (two levels of significance, p-value = 0.0012) in the amount of inflammatory specific signal detected in the demsoplakin-deficient samples respect to the WT reference.

As the graph tells us, the DH pool showed an inflammatory specific signal that was doubled respect to the WT animals. The difference is clear in both images, where L-plastin specific spots (in the circles) can be easily discriminated from the background and superimposed in the bright field and fluorescent channels.

4.3. *Heart chambers dilation.*

To further improve the specificity, and relevance, of the previous morphological characterization of the cardiac region, green heart transgenic embryos (3dpf) were analyzed to assess the level of dilation of the heart's chambers in the two conditions – overlooking, this time, the dimensions of the whole cardiac region. In the figure below, representing the merged images between the bright-field and the fluorescent channel, we can see that the DH mutant line displayed a heart volume that was overtly larger than the WT condition.

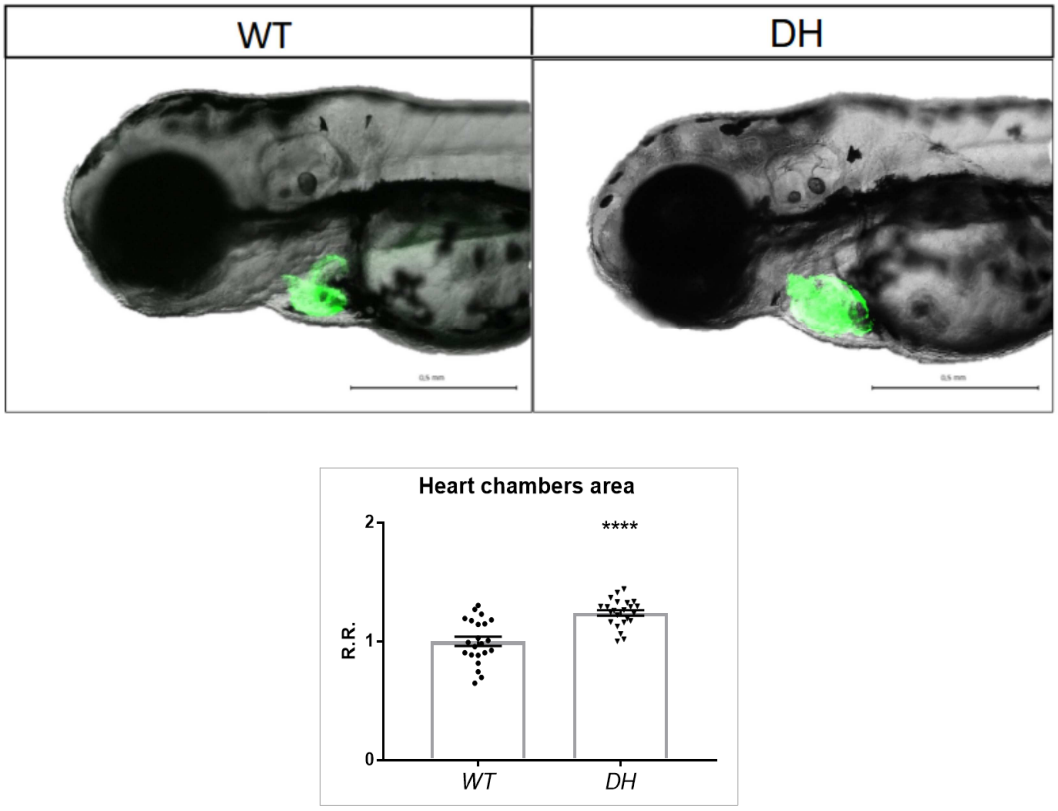

Figure 4.4. ***Heart chambers dilation in the double-heterozygous condition.***
Qualitative and quantitative analysis of the DH heart dilation. All embryos are in lateral view, anterior to the left. Number of samples n = 22. **** = p-value < 0.0001. Test: unpaired t-test with α = 0.05. R.R. = relative ratio.

This dilation was consequently estimated to be both highly significant (four level of significance, after a parametric t-test statistical analysis; p-value < 0.0001) and consistent with the cardiac region analysis, with a mean dilation of about 30% (*i.e.* DH hearts were ≈ 30% higher than the WT) (see graph in Figure 4.4.).
Looking at the merged images in the example, we can also notice that the dilation of the ventricle (the upfront chamber) is so high, in the DH line, that the two chambers are no longer distinguishable, differently from the WT case.
The ventricle dilation, whose fluorescent signal thus appears to be completely predominant, was then further confirmed by a supplementary analysis that was carried out on the adult fishes.
In parallel with the analysis on the green heart embryos, in fact, a pool of adult hearts was extracted (for both condition) and consequently analyzed for significant differences in their ventricular areas (see Figure 4.5).

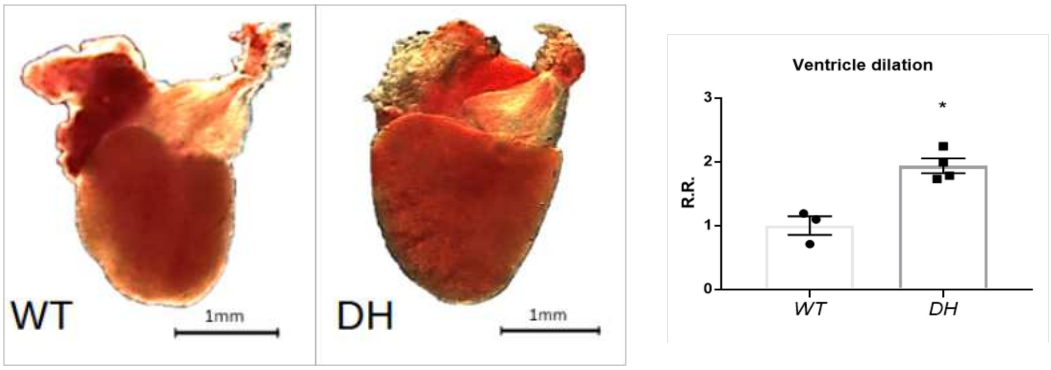

Figure 4.5. ***Adult hearts and ventricle area comparison.*** Images on the left: extracted adult hearts representatives of the WT and DH condition. Chart on the right: quantification of ventricular dilation in the DH line. Number of samples n = 3, n = 4. * p-value < 0.05. Test: unpaired t-test with α = 0.05. R.R. = relative ratio.

Our decision to focus specifically on the ventricles was due to the clinical manifestation of AC.
Being its pathogenesis specifically affecting the ventricles, it appeared more strategic to focus directly on them also in the zebrafish model, willing to consider the anatomical district where the majority of damages concentrates. According to this, Figure 4.5. shows that the DH heart displayed an evident chamber dilation respect to the WT condition, with a mean surface that was two times the normal one (p-value 0.004).

4.4. Birefringence analysis.

To better understand whether the structural damages induced by the demsoplakin mutation were specifically located in the sole cardiac region, we performed a birefringence assay to exclude a possible involvement of the skeletal muscles.
In Figure 4.6. we plotted the result of the analysis, with the data of two pools of larvae (WT and DH) that are both represented as mean of intensity – skeletal muscles brirefringence intensity – normalized for the samples length.

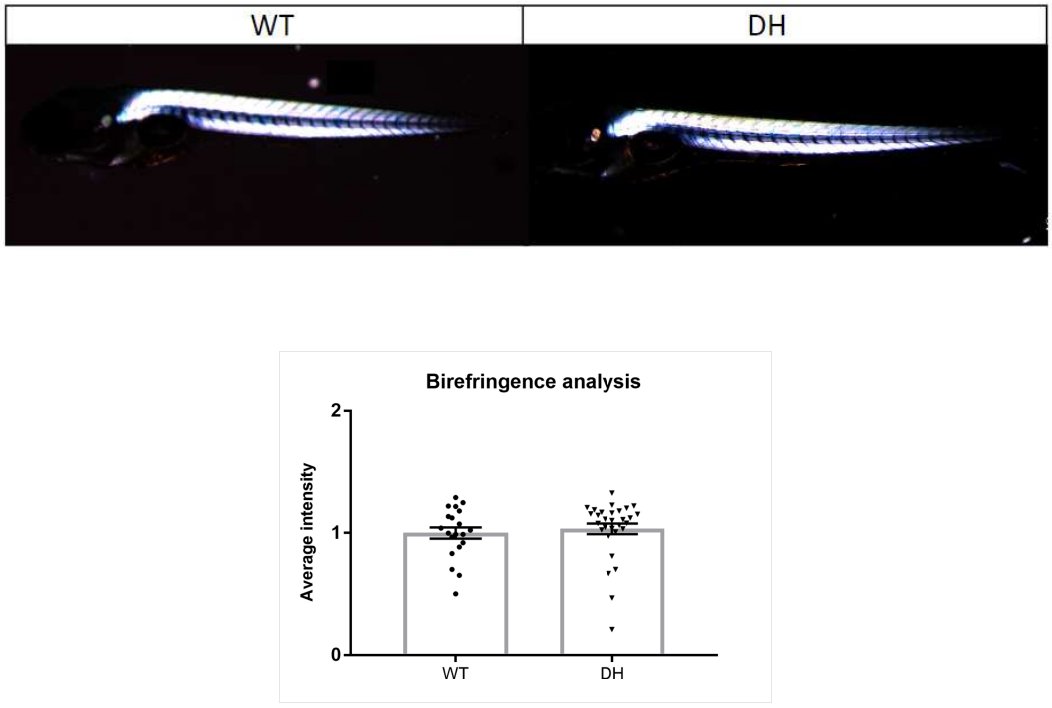

Figure 4.6. ***Birefringence analysis.*** Average intensities of the birefringence signal are indicative of the level of damages in the skeletal muscles of the two experimental condition. All larvae (5dpf) are in lateral view, anterior to the left. Number of samples n = 25. Test: unpaired t-test with α = 0.05.

According to our results, as can be also appreciated in the representatives images, there were no significant differences in the mean birefringence signal of the two pools (p-value of 0.6058), suggesting that the two pools are practically identical, with no evident fiber disorganization in the skeletal muscles.

4.5. *Physical training (larval stage).*

The methyl-cellulose physical training was performed, as previously explained, for 10 consecutive days in Petri dishes, counting the number of deaths per condition on a daily basis.
In Figure 4.7., below, the results – plotted as percentage of survival at a given date – show the differences, in terms of slopes of the curves, of each of the four conditions (WT rest; WT training; DH rest; DH training).

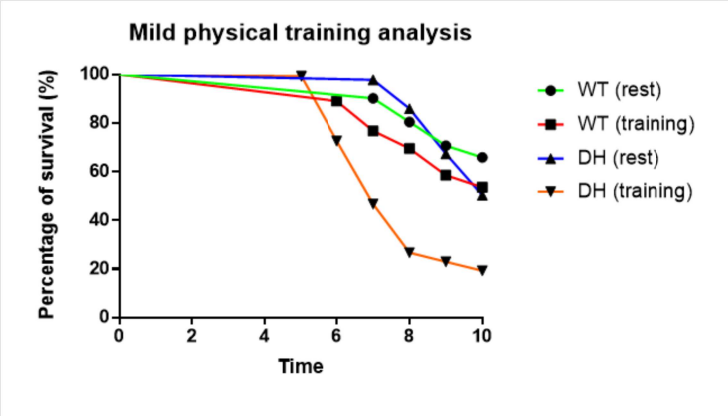

Figure 4.7.

Mortality rates estimates for the methyl-cellulose training.

Kaplan - Meier curves of the different genotypes describe the level of resistance of the considered pool. Number of samples n = 100. Test = Log – Rank (Mantel-Cox) test.

Looking at the different curves, we can immediately appreciate that there is a difference, in the mortality trend, between the resting and the training condition, with the trained larvae that – independently from their genotype – showed a faster decrease respect to the control (rest) counterparts.
According to this, every pairwise comparison (ctrl - training) resulted to be, at different levels, statistically significant, with the only exception represented by the WT training vs the DH resting pools (red and blue lines in the graph, respectively).
In particular, the WT genotype showed a reduction of 12% when subjected to the training protocol (54 % vs 66 % of survival at the end of the analysis) and the date of the first recorded event (death) was shifted of 1 day between the two pools.
The DH trained larvae, on the other hand, did not show any kind of anticipation, but the overall decrease of their pool was significantly higher than the previous comparison, with a final survival rate (19%) that was a 30% lower than the control condition (50%). Furthermore, if we compare this result with the death

rate of the DH at rest at 30 days (Figure 3.8), we can appreciate that the two condition are almost identical, thus suggesting that the training protocol is indeed accelerating the mortality process.
If we then compare the two different genotypes, this difference becomes even more evident and informative, since, in this case, also the comparison between the trained pools (WT trained vs DH trained) is statistically relevant, with four level of significance and a p-value < 0.0001 (not shown in the graph).

4.6. Physical training (adult stage) and histological analysis.

Histological analysis was performed on trained and control (rest) animals to assess the level of morphological differences, in the cardiac region, induced by an intensive kind of physical effort.
Figure 4.8. shows the comparisons, at different magnifications, of the histological sections obtained from WT and desmoplakin-deficient pools.
The first image, in particular, shows all the experimental conditions (WT resting and training, DH resting and training) of the training protocol, with overt anatomical differences that can be appreciated in the ventricles of the two genotypic conditions.
First of all, the overall ventricular area of the DH line resulted significantly dilated and abnormally shaped, with a slight, yet significant, wall thickening (arrows in the image) and a global disorganization in the trabecular arrangement that specifically characterizes ventricle's myocytes.
Secondly, blood vessels dimensions appeared generally increased, with individual cells (erythrocytes or leukocytes, both nucleated in zebrafish) that can be easily distinguished inside the enlarged lumen.
Lastly, adipocytes accumulation is also visible in the peripheral region of the DH ventricle (see the 40 x detail), with the infiltration site close to the ventricular wall.
The prevalence, and entity, of these pathological signatures becomes even more important if we consider the trained pool, where the DH line showed an increase both in the number of infiltrated adipocytes and in the disorganization of the trabecular network.
Conversely, the WT animal subjected to the training protocol displayed only a lighter disorganization of the trabecular network, with no sign of dilation, adipocytes accumulation or wall thickening.

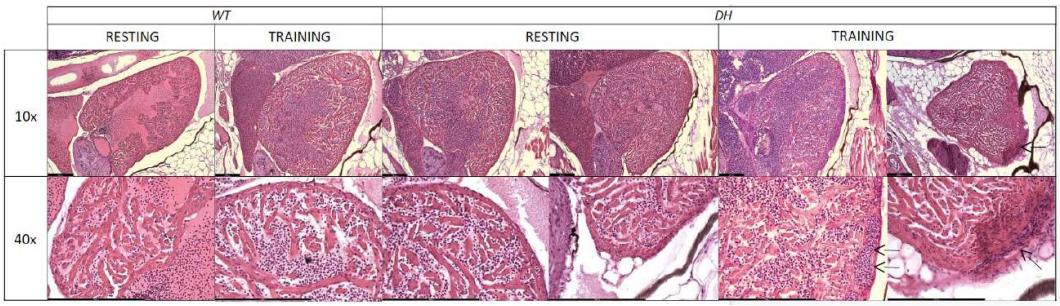

Figure 4.8. ***Ventricles histological sections of trained and resting fishes.*** Arrows indicates wall thickening and blood vessels dilations. Adypocytes infiltrations sites can be distinguished both in the DH rest and the DH trained condition, with a significant increase in the number of infiltrated cells in the DH trained animal (10 x magnification).

Furthermore, comparing the DH images in Figure 4.8 and Figure 4.9 (below), we can notice that the entity of the anatomical changes (vessels dilation, trabecular disorganization and adipocytes infiltration) provoked by a 3-month training regime (from 3 mpf to 6 mpf) are completely similar (if not identical) to those displayed by a 9 months old not trained DH condition (Figure 4.9), suggesting that the training protocol is, has expected, dramatically accelerating the progression and worsening of the pathological condition.

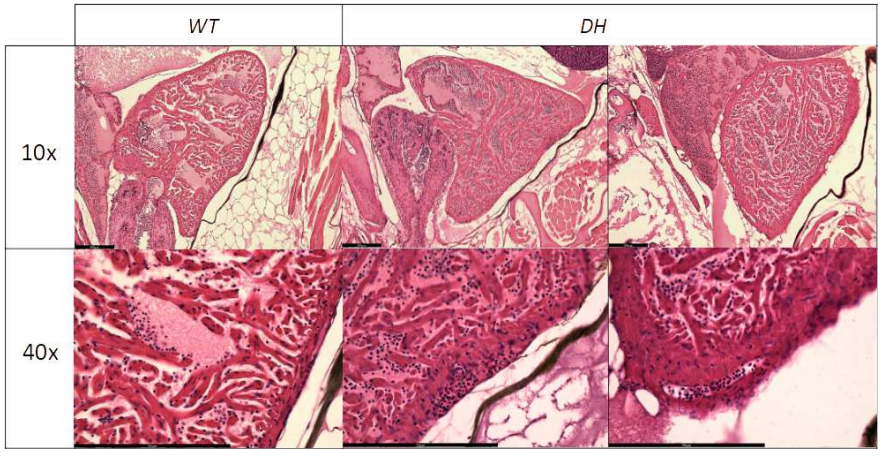

Figure 4.9. ***WT and DH ventricles of 9-month old fishes.*** Both images are representatives of resting animals, highlighting the anatomical abnormalities of the DH condition, with an aberrant cardiac shape, wall thickening, blood vessels dilation and adypocyte accumulation.

4.7. ***Drug treatments***.

4.7.1. *Wnt pathway modulation*.

Pharmacological modulation of the Wnt/β-catenin pathway was assessed through the quantification of signal intensity in Wnt responsive GFP transgenic 3dpf embryos (*Tg(7xTCF-Xla.Siam:GFP)*). The results are summarized in Figure 4.10., where each intensity value is normalized to the area of the considered region, after background noise subtraction.

According to the scatter plot, each experimental condition was found as significantly different from the WT control, with the statistical confidence that ranged from two to four levels of significance in the pairwise comparisons.

That said, a dutiful consideration has to be made for the DH + SB pool, which is clearly distinguished from all other pools in the scatter plot.

First of all, as in the previous case, the level of significance of the statistical difference between the SB-treated embryos and the WT condition is lower than all the other comparisons, with an estimated p-value of 0.0060 after the ANOVA parametric analysis.

Secondly, the meaning of this statistical difference – difference from the WT pool – is completely opposite respect to the other cases.

Looking at the mean values of intensities, in fact, we can notice that the Relative Intensity (R.I.) of the DH + SB pool resulted to be higher – not lower – than the WT reference, with an estimated difference of 0.16 (16%) in their final numbers.

Focusing on the second kind of treatment, instead, we can see that the DH + XAV pool resulted, once again, the worst in terms of phenotype display, with a level of GFP fluorescent signal that was almost 70% (67.7%) reduced respect to the WT condition. This huge difference between the DH + XAV and the DH + SB pools accounts for the opposite effect that the two drugs exert on the canonical Wnt signal; even considering the difference with the DH control condition, which, as the scatter plot shows, displayed a mean level of intensity more than 30% (± 30%) different from both the pharmacological conditions (p-values < 0.0001).

The differences in the GFP expression can be also appreciated, visually, in the first image of Figure 4.10., where representatives examples of the mean Wnt activity *per condition* are compared for signal intensities in the head and in the cardiac region of the considered individual, with the heart's valves that are highlighted as a clear Wnt-expressing anatomical district.

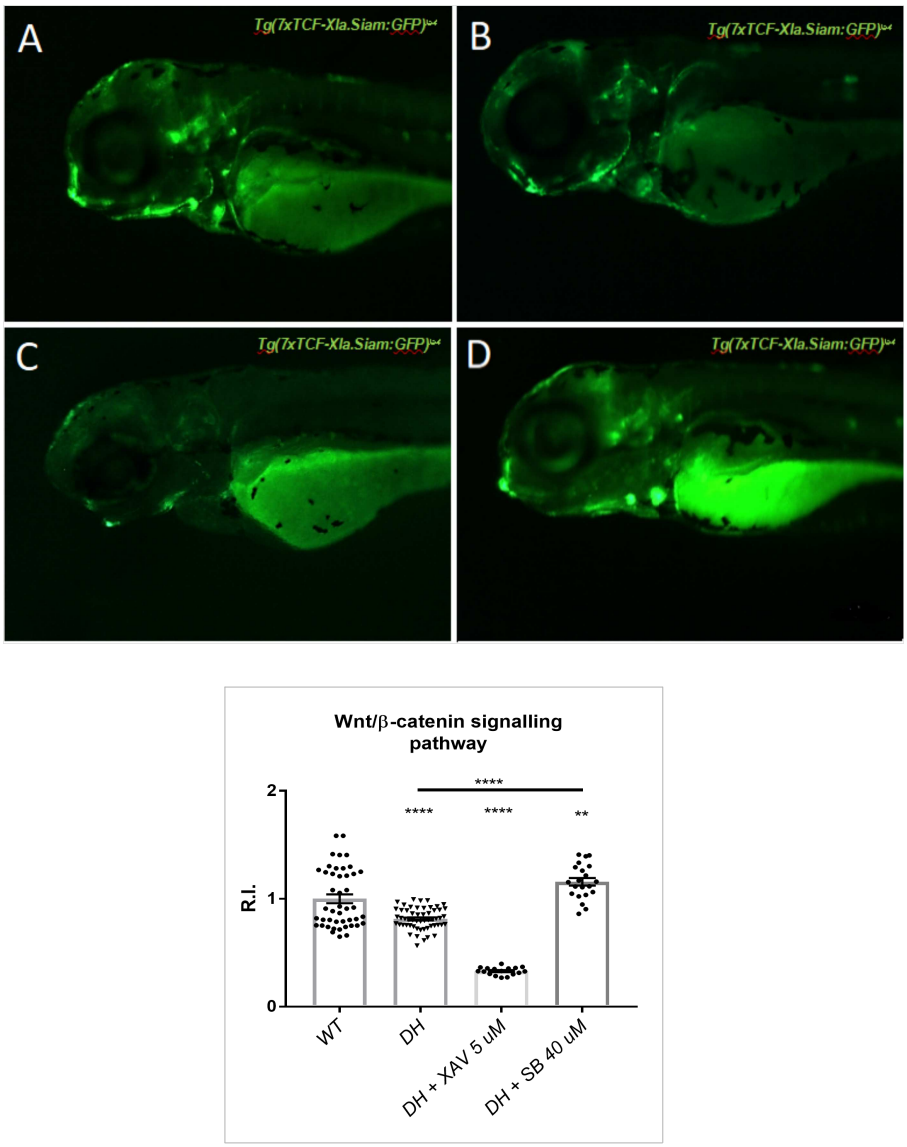

Figure 4.10. ***Wnt canonical signaling in the different experimental conditions.*** Top images: Wnt/β-catenin responsive GFP fluorescent signal in 3dpf transgenic embryos: A) WT B) DH C) DH + XAV 5 µM D) DH + SB 40 µM. All samples are in lateral view, anterior to the left. Bottom chart: Scatter plots of fluorescence intensities in the different pools. Number of samples n = 35. ** p-value < 0.01, *** p-value < 0.001, **** p-value < 0.0001. Test: one way ordinary ANOVA with α = 0.05 and multiple comparisons. R.I. = relative intensity.

4.7.2. Morphological alterations and heart rate estimate.

Pharmacological assays were performed on wild-type and DH mutant embryos to assess the effects, on the pathological phenotype, of the XAV939 and the SB216763 drugs.

In figure 4.11., the percentages of the morphological altered embryos (3dpf) after 48 hrs treatment are compared with the control (non-treated) animals. As in the previous characterization, the WT pool resulted to be the less affected pool, with only 9% of embryos that displayed the previously mentioned cardiac alterations (edemas, dilation etc.)

Conversely, the DH line subjected to the 5 µM XAV treatment showed the worse phenotype, with most of the individuals (96%) which presented at least one overt abnormality.

The most interesting part of the analysis, though, regards the comparison between the remaining two pools: the DH control and the DH SB treated.

Looking at the graph, we can notice that the proportions of altered fishes in these two pools are only slightly influenced by the SB drug, with just a 6 % reduction (from 22 to 16%) in the overall abnormalities displayed after the pharmacological treatment.

Yet, this slight difference is quite significant, and informative, since it demonstrates that the SB drug is indeed having an effect (even though limited) on the overall display of the cardiac morphological alterations.

Moreover, if we then focus exclusively on just one of the parameters considered for the overall morphological analysis, the cardiac region dilation, the effect of the SB drug acquires an even greater importance.

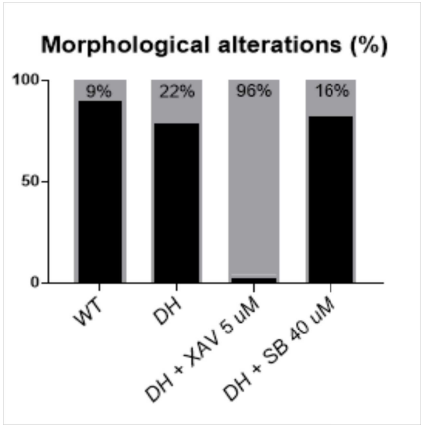

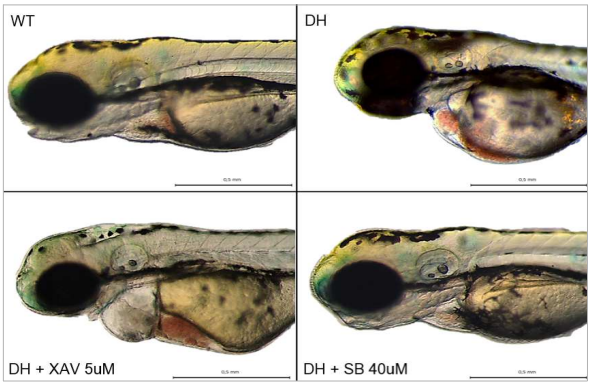

Figure 4.11. ***Morphological characterization of treated larvae*.** Chart: Percentages of altered cardiac regions in treated and untreated embryos's pools. Images: Representatives examples of the mean morphological condition in the different genotypical and experimental conditions. All embryos (3dpf) are in lateral view, anterior to the left. Number of samples n = 100.

Figure 4.12. is explicative in this sense, where the scatter plots of the cardiac region dimensions are represented in combination with the aforementioned normalization – and developmental – factors (body length and eye size).
In particular, focusing on the third graph (cardiac region size) we can observe that the WT and the DH SB treated scatter plots are almost identical, in terms of shape, average value and standard deviation, with the set of experimental points (measurements) that are thus compactly and uniformly distributed around the mean.
On the other hand, as in the previous case, the DH pool treated with XAV displayed the worst possible phenotype, with an estimated mean dilation that was more than two times higher than the DH control pool (pairwise comparison p-value < 0.0001), even considering the high level of variability found within the pool.
The same level of significance (p-value < 0.0001) was found also in the last pairwise comparison, with the DH *vs* DH SB pools that resulted, conversely to the overall morphological analysis (Figure 4.11.), way more different in the display of such edematous dilation.
Figure 4.12., eventually, is also accounting for the developmental delay's rescue that was observed in the DH + SB pool, in which both of the considered parameters (body length and eye size) resulted non significantly (ns) different from the WT normal condition.
Following the initial mutant lines' characterization, a parallel analysis of the heart rate at 5 dpf was also conducted during the pharmacological assay (see the bottom chart of Figure 4.12). In this case, as the scatter plot suggests, all DH mutant lines resulted significantly different from the WT condition, whose mean heart rate was once again estimated to be around 170 beats per minute (at 5 dpf).
According to this point, though, we have to notice that the heart rate of DH + SB line, despite being quite different from the WT one (four levels of significance, p-value < 0.0001) showed an evident increase respect to the initial, control condition, with a mean value that changed from 135 to 150 beats per minute after the drug treatment.
Furthermore, if we then consider the difference between the DH control and DH treated pools, four levels of significance in the pairwise comparison, we have a compelling evidence of the rescue experienced by the DH + SB larvae. Eventually, the hart beats' analysis highlighted another variation in the differences between the pools, since both the DH control and the DH + XAV larvae displayed the same beats per minute mean value (≈135), with an estimated p-value > 0.9999.

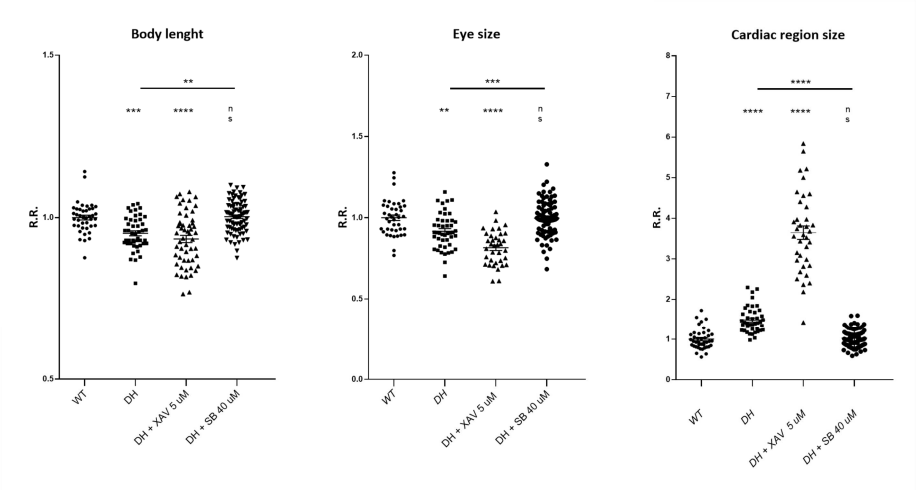

Figure 4.12. ***Drug treatment effect on developmental and cardiac parameters.*** Top charts: Developmental factors and cardiac region dilation estimates before and after treatment. Bottom chart: Heart rate (beats per minute) estimates in 5 dpf larvae subjected to the pharmacological assay. Number of samples n = 65. ns = non significant, ** p-value < 0.01, *** p-value < 0.001, **** p-value < 0.0001. Test: one way ordinary ANOVA with α = 0.05 and multiple comparisons.

4.7.3. Mortality (survival) assay.

WT, double heterozygous (ctrl) and DH + 40 uM SB mutant larvae were analyzed for 30 days to assess the level of changes in the mortality rates after the drug treatment.

The resulting Kaplan - Meier curves are reported in Figure 4.13., underlining an evident difference between the DH ctrl and the DH treated pools, with the latter that showed a significant increase in the survival rate and an overall survival trend which was highly similar – until 18 dpf almost identical – to the WT reference group.

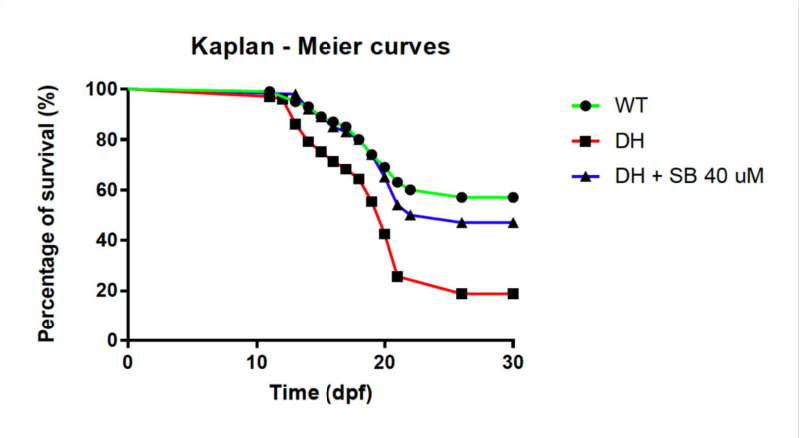

Figure 4.13. ***Kaplan – Meier curves of the dh mutant larvae before and after the SB treatment.*** Percentages of survivals of WT (green) DH control (red) and DH treated larvae (blue) were determined on a daily basis by counting the numbers of registered of events (deaths) per condition. Number of samples n = 100. Test: Log -Rank (Mantel – Cox) test.

In particular, the percentages of survivals at 30 days differed, between the WT and the SB treated larvae, of just about 10 points (57 % vs 47 %, respectively), while the double heterozygous control pool ended up with a number three times lower (19%) than the WT pool, confirming the previous mortality rate and highlighting a non casual discrepancy with the treated counterpart (p-value < 0.0001). Furthermore, if we consider the overall trend of the curves, we can notice that the slope of the DH line (in red) was, even in the first days, when the first deaths started to appear, evidently higher than the others, and the magnitude of this difference progressively increased with the progression of the analysis.

4.7.4. Training.

Five days of 1% methyl-cellulose training were performed on treated and untreated pools to study the effect of the SB drug on the resistance of the double heterozygous mutant larvae.

The Kaplan - Meier curves of Figure 4.14. clearly show, as in the previous methyl cellulose training discussion, an evident difference between the resting (control) and the training conditions, with the control pools that ended the analysis without experiencing any fatality (100 % of survivors).

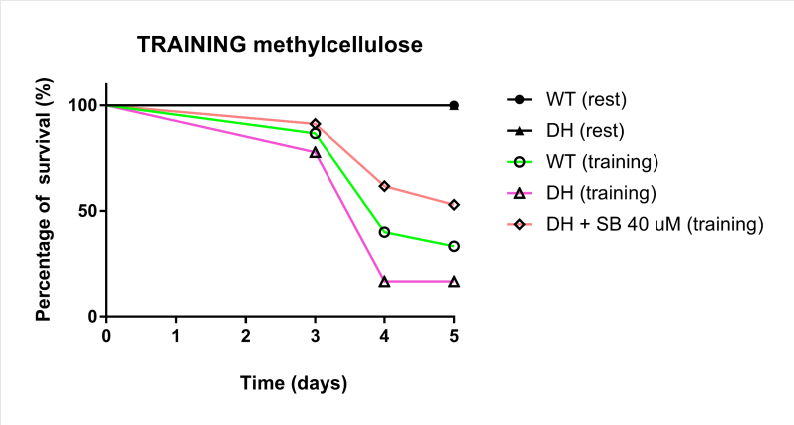

Figure 4.14. ***Survival rates of the different pools in a physical training regime.*** Kaplan - Meier curves of each experimental conditions were estimated as in the previous examples. SB drug was constantly changed throughout the analysis to improve pharmacological efficacy. Number of samples n = 20. Test: Log Rank (Mantel – Cox) test.

More interesting is the comparison between the trained pools, which, despite showing the same kind of death trend, started at 3 dpf and continued – with increased slopes – in the following days, showed significant differences in their final number of survivors. In particular, focusing on the WT methyl-cellulose pool (green line) – which resulted to be not significantly different from the other two DH conditions – we can notice that it displayed a survival trend in between the curves of the corresponding mutant lines; rest and trained.

This result, as we can understand, is quite interesting, since it implies that the SB treated larvae (red line) – which ended up with the highest number of survivors (53%) – manifested an overall resistance, to the physical stress, even greater than the WT reference pool.

If we then look at the difference, in terms of deaths per condition, between the treated and the untreated DH pools, this consideration becomes even more important, with a final number of survivors that was more than two times higher in the SB methyl-cellulose larvae respect to the control, untreated counterpart, as confirmed by the two levels of significance of the pairwise comparison (p-value 0.0054).

5. DISCUSSION

The study of Arrhythmogenic Cardiomyopathy is an intricate process, which necessarily requires a multilateral kind of approach – from the initial characterization (genetical and histological) of the samples to the direct targeting of the signaling interplay which is at the basis of the fibro-fatty substitution (Yuan *et al.*, 2021).

Our work, integrating the discoveries of Asimaki and colleagues (Asimaki *et al.*, 2014), demonstrates the potentialities of *Danio rerio* as a disease model for the study of AC, investigating the role of the canonical Wnt pathway in the pathological progression and exploring the efficacy of the SB216763 drug as a new potential pharmacological treatment.

First of all we verified the dysregulation of the Wnt/β-catenin signal through a real-rime (qPCR) and an *in vivo* fluorescent characterization of the desmoplakin deficient larvae (Figures 3.7, 4.10), finding, in both cases, a significant down-regulation of the canonical pathway.

Of note, the double heterozygous (DH) mutant line showed a higher decrease in the overall signal expression, with a level of *ccnd1* mRNA that was significantly lower than *c-myc* mRNA in the other mutant lines.

This result, the down-regulation of the Wnt signal, is fully consistent with the general hypothesis about Wnt dysregulation within the pathological context of AC, in which the destabilization of the desmosomal complex is impacting β-catenin activity through the release of y-catenin (plakoglobin) (Garcia-Gras *et al.*, 2006) (Calore *et al.*, 2019).

However, the cytosolic accumulation (and/or changes in expression) of plakoglobin was not directly assessed in our experiments due to the lack of suitable/working antibodies.

The down-regulation of the Wnt signaling was accompanied by a developmental delay of the mutant larvae, with an evident reduction in both the parameters normally considered as benchmarks of the zebrafish growth: the body length and the eye's size (Figure 3.4, 4.12).

Interestingly, this decrease in the overall dimensions of the fish – a feature that could have also impacted the sizes of the organs – did not applied in the case of the cardiac region, which, on the contrary, displayed an overall surface that was significantly dilated respect to the WT condition (Figure 3.4, 4.12). This dilation was indeed linked with the structural destabilization of the cardiac muscle, which,

as a consequence, together with the down-regulation of the Wnt signal, produced a series of morphological alterations, from the accumulation of fluids (edemas) to blood effusions episodes, eventually resulting in the general enlargement observed for the cardiac region.

More important, though, is the association between the cardiac region dilation and the ventricular area, with the chambers that resulted dilated both in the larvae and in the adult mutant lines (Figure 4.4, 4.5).

This result – the dilation of the heart – is perfectly consistent with AC progression in humans, with some cases that have in fact been linked with a dilation either in the right, in the left or in both ventricles (Sen-Chowdhry *et al.*, 2004) (Igual *et al.*, 2011).

Furthermore, if we compare the level of cardiac dilation displayed at the two experimental time points, at larval stage and in the adult animals, we understand that the progression of the disease is indeed linked, even in the zebrafish model, with the worsening of its pathological condition, with a heart surface that was more than doubled in the adult hearts.

The same conclusion can be inferred from the histological analysis, where, at rest, the 9 months old DH samples presented an overall condition that was significantly worse than the 6 months old ones (Figure 4.8, 4.9).

Considering, then, the intrinsic variability of the cardiac region alterations at larval stage – that either co-existed or were differently evident in distinct animals – and the proportions of samples which displayed such kind of phenotypes (≈ 25/30%) (Figure 3.3, 4.11), we have a faithful reconstruction of the variable penetrance that characterizes AC (Pinamonti *et al.*, 2014).

Seen the recent discoveries about inflammation, as a factor related with AC pathogenesis (Asatryan *et al.*, 2021) (Yuan *et al.*, 2021), the detection of inflammatory specific cells was then assessed through an immunofluorescence analysis, in which the demsoplakin-deficient larvae displayed an overall signal intensity (L-plastin specific) that was more than doubled, in the cardiac region, respect to the WT condition (Figure 4.3.).

This result is confirming that the pathological context of Arrhythmogenic Cardiomyopathy is indeed characterized by an increase in inflammatory specific markers, whose appearance can be triggered both by the destabilization of the desmosomal complex (through the alteration of the aforementioned and other signaling pathways, such as the NF-kB signal) (Yuan *et al.*, 2021), and, at least in the zebrafish model, the blood effusions episodes, which, by themselves, increase

the possibility to find inflammatory-related blood cells (*i.e.* leukocytes) inside and all around the cardiac region.

Another important confirmation was obtained, once again, from the histological samples, where the presence of adipocytes infiltration in the ventricle's area emerged, above all, as a clear marker of AC onset in the mutant condition (Figure 4.8). On the other hand, though, the subtle thickening of the ventricular wall observed in the DH samples can be referred to as an interesting difference with the wall-thinning generally observed in most of the AC cases (Corrado *et al.*, 2017).

This discrepancy may be attributed to the peculiarity of the zebrafish model, which, having a very efficient heart's regeneration capability (Beffagna, 2019), could have increased the ventricle thickness as a compensatory response for the structural destabilization of the myocardium.

Related to this zebrafish feature, then, the missed observation – in the histological samples – of the fibrogenesis phenomenon, still remains, together with the lack of information about arrhythmia episodes, one of the main criticisms of our model.

Even considering these inconsistencies, though, the relevance of our double-heterozygous desmoplakin-deficient zebrafish mutant for AC modeling, and study, was still strongly supported – among all the other evidences – by the training protocols, which, both in the larvae and the adult animals resulted in the evident worsening (and acceleration) of the pathological phenotype due to the sole cardiac dysfunction (Figure 4.7, 4.8), as suggested by the birefringence analysis (Figure 4.6), which excluded skeletal muscle fiber disorganization.

Having demonstrated the potentialities of the DH model, our focus shifted then to what can be considered the real aim of this thesis: the rescue of AC pathological signatures through the modulation of the canonical Wnt signal. The potentialities of the SB drug for the treatment of the AC were previously identified by Asimaki's team through a pharmacological screening carried out on a different desmoplakin-deficient zebrafish line (Asimaki *et al.*, 2014). Nevertheless, Asimaki's work was only hypothesizing – at the end – the putative reversibility of the disease, noticing the effect of the SB drug in the prevention of the action potential remodeling on both zebrafish larvae and *in vitro* cultured rat cardiac myocytes.

Our work demonstrate such reversibility at several levels, from the morphological to the molecular one. Specifically, as illustrated in the final part of the results, the recovery of the Wnt signal down-regulation (Figure 4.10) has been followed by an improvement of all the considered pathological parameters; from the overall dimensions of the cardiac region, whose dilation was drastically reduced with the

SB drug (Figure 4.12), to the survival rate, which, both in trained and rest regimes showed a significant increase under the pharmacological treatment (Figure 4.13, 4.14).

Furthermore, the direct effect of the SB drug on the heart's function – only indirectly postulated in Asimaki's work – has been demonstrated through the analysis of the heart rate, which, in the same way, resulted closer to the WT condition in the pool of treated larvae (Figure 3.5, 4.12). To conclude, our work, continuing Giuliodori's one (Giuliordori *et al.*, 2018) demonstrates the suitability of *D.rerio* for the dissection, and modeling, of the Arrhythmogenic Cardiomyopathy, further reinforcing the evidences in favor of the SB drug as a new, potential therapeutic approach, capable of limiting – if not abolish – the detrimental effects of the pathological progression through the inhibition of the GSK3 activity (Chelko *et al.*, 2016).

However, despite being already approved for the treatments of neuronal-related diseases (Rao *et al.*, 2019), other supplementary analyses are necessary to confirm the beneficial role of the SB drug in the case of AC, considering its recent discovery and its potentially carcinogenic effects on a key cell signaling pathway (*i.e.* the canonical Wnt signal).

6. CONCLUSIONS AND FUTURE PERSPECTIVES

Our work clarifies the role, nature and impact of the Wnt pathway dysregulation in the pathogenesis of Arrhythmogenic Cardiomyopathy, pointing out its pharmacological modulation as a key factor for the recovery – and limitation – of the major symptoms.

However, to further improve the consistency of our results and the goodness of our model, other experiments could be pursued. For this reason, we are currently planning to test the SB drug in the adult animals as well, trying to reproduce the beneficial effects observed at the larval stage for the cardiac alterations present in the histological samples – of particular interest would be the recovery of the adypocytes accumulation, which could be indicative, in qualitative terms, of the disease regression.

Linked to this purpose, it would be also interesting to perform some electrophysiological experiments on the WT and mutant conditions, assessing 1) whether there is an effective impairment of the cell conductivity, 2) at what level (which grade of magnitude) such impairment is happening, further investigating,

and dissecting, the mechanism that – as the reduced hart rate suggests – is impacting the proper functioning of the cardiac muscle in the presence of a structural destabilization. According to this, the detection of arrhythmia episodes, both at larval and adult stage, would be extremely important and interesting, finding out whether there is a difference (as expected) between the DH and the WT conditions.

Lastly, we are also considering to test the efficacy of the SB drug for the recovery of the inflammatory-specific markers, performing the immunofluorescence protocol both at larval and adult stage, which allows to better discriminate the anatomical localization (and cardiac infiltration) of the L-plastin^{+} immune cells.

BIBLIOGRAPHY

1. Akdis D., Saguner A. M., Shah K., Wei C., Medeiros-Domingo A., von Eckardstein A., Lüscher T. F., Brunckhorst C., Chen H., Duru F. *Sex hormones affect outcome in arrhythmogenic right ventricular cardiomyopathy/dysplasia: from a stem cell derived cardiomyocyte-based model to clinical biomarkers of disease outcome*. European heart journal, 2017, 38(19): pp 1498-1508.

2. Arunachalam *M., Raja M., Vijayakumar C., Malaiammal P., Mayden R. L. Natural History of Zebrafish (Danio rerio) in India.* Zebrafish, 2013, 10(1): pp 1-14.

3. Asatryan B., Asimaki A., Landstrom A. P., Khanji M. Y., Odening K. E., Cooper L. T., Marchlinski F. E., Gelzer A. R., Semsarian C., Reichlin T., Owens A. T., Chahal C. A. A. *Inflammation and Immune Response in Arrhythmogenic Cardiomyopathy: State-of-the-Art Review. Circulation, 2021, 144(20): pp 1646-1655.*

4. Asimaki A., Kapoor S., Plovie E., Arndt A., Adams E, Liu Z. Z., James C. A, Judge D. P., Calkins H., Churko J, Wu J. C., MacRae C. A., Kleber A. G., Saffitz J. E. *Identification of a New Modulator of the Intercalated Disc in a Zebrafish Model of Arrhythmogenic Cardiomyopathy.* Science Translational Medicine, 2014, 6(240):240ra74.

5. Basso C., Corrado D., Marcus F. I., Nava A., Thiene G. *Arrhythmogenic right ventricular cardiomyopathy.* The Lancet, 2009, 373(9671): pp 1289-300.

6. Beffagna G. *Zebrafish as a Smart Model to Understand Regeneration After Heart Injury: How Fish Could Help Humans.* Frontiers in Cardiovascular Medicine, 2019, 6: pp 107.

7. Bomma C., Ruterberg J., Tandri H., Nasir K., Roguin A., Tichnell C., Rodriguez R., James C., Kasper E., Spevak p., Bluemke D. A., Calkins H. *Misdiagnosis of Arrhythmogenic Right Ventricular Dysplasia/Cardiomyopathy.* Journal of Cardiovascular Electrophysiology, 2004, 15: pp 300-306.

8. Calore M., Lorenzon A., De Bortoli M., Poloni G., Rampazzo A. *Arrhythmogenic cardiomyopathy: a disease of intercalated discs.* Cell Tissue Research, 2015, 360(3): pp 491-500.

9. Calore M., Lorenzon A., Vitiello L., Poloni G., Beffagna G., Dazzo E., Polishchuk R., Sabatelli P., Doliana R., Carnevale D., Lembo G., Bonaldo P., De Windt L., Braghetta P., Rampazzo A. *A novel murine model for arrhythmogenic cardiomyopathy points to a pathogenic role of Wnt/β-catenin signaling and miRNA dysregulation.* Cardiovascular Research 2019, 115(4): pp 739-751.

10. Chelko S. P., Asimaki A., Andersen P., Bedja D., Amat-Alarcon N., DeMazumder D., Jasti R., MacRae C. A., Leber R., Kleber A.G., Saffitz J. E., Judge D. P. *Central role for GSK3β in the pathogenesis of arrhythmogenic cardiomyopathy.* The Journal of Clinical Investigation (JCI), 2016, 1(5):e85923.

11. Corrado D., Basso C., Judge D. P. *Arrhythmogenic Cardiomyopathy.* Circulation Research, 2017, 121(7): pp 784-802.

12. Delmar M., McKenna W. J. *The Cardiac Desmosome and Arrhythmogenic Cardiomyopathies: From Gene to Disease*. Circulation Research, 2010, 107(6): pp 700-14.

13. Facchinello N., Tarifeño-Saldivia E., Grisan E., Schiavone M., Peron M., Mongera A., Ek O., Schmitner N., Meyer D., Peers B., Tiso N., Argenton F. *Tcf7l2 plays pleiotropic roles in the control of glucose homeostasis, pancreas morphology, vascularization and regeneration.* Scientific Reports, 2017, 7(1): pp 9605.

14. Garcia-Gras E., Lombardi R., Giocondo M. J., Willerson J. T., Schneider M. D., Khoury D. S., Marian A. J. *Suppression of canonical Wnt/beta-catenin signaling by nuclear plakoglobin recapitulates phenotype of arrhythmogenic right ventricular cardiomyopathy.* The Journal of Clinical Investigation (JCI), 2006), 116(7): pp 2012-21.

15. Garrod D., Chidgey M. *Desmosome structure, composition and function.* Biochimica and Biophysica Acta (BBA) – Biomembranes, 2008,1778(3): pp 572-87.

16. Giuliodori A., Beffagna G., Marchetto G., Fornetto C., Vanzi F., Toppo S., Facchinello N., Santimaria M., Vettori A., Rizzo S., Della Barbera M., Pilichou K., Argenton F., Thiene G., Tiso N., Basso C. *Loss of cardiac Wnt/β-catenin signalling in Desmoplakin-deficient AC8 zebrafish models is rescuable by genetic and pharmacological intervention.* Cardiovascular Research, 2018, 114(8): pp 1082-1097.

17. Igual B., Zorio E., Maceira A., Estornell J., Lopez-Lereu M. P., Monmeneu J. V., Quesada A., Navarro J., Mas F., Salvador A. *Arrhythmogenic cardiomyopathy. Patterns of ventricular involvement using cardiac magnetic resonance.* Revista Española de Cardiología, 2011, 64(12): pp 1114-22.

18. Li D., Liu Y., Maruyama M., Zhu W., Chen H., Zhang W., Reuter S., Lin S. F., Haneline L.S., Field L. J., Chen P.S., Shou W. *Restrictive loss of plakoglobin in cardiomyocytes leads to arrhythmogenic cardiomyopathy.* Human Molecular Genetics, 2011, 20(23): pp 4582-96.

19. Li J., Swope D., Raess N., Cheng L., Muller E. J., Radice G. L. *Cardiac tissue-restricted deletion of plakoglobin results in progressive cardiomyopathy and activation of {beta}-catenin signaling*. Molecular Cell Biology, 2011, 31(6): pp 1134-44.

20. Lieschke G. J. and Currie P. D. *Animal models of human disease: zebrafish swim into view.* Nature Reviews Genetics, 2007, 8: pp 353–367.

21. Lorenzon A., Calore M., Poloni G., De Windt L. J., Braghetta P., Rampazzo A. *Wnt/β-catenin pathway in arrhythmogenic cardiomyopathy.* Oncotarget, 2017, 8(36): pp 60640-60655.

22. Ma L., Wang X., Jia T., Wei W., Chua M. S., So S. *Tankyrase inhibitors attenuate WNT/β-catenin signaling and inhibit growth of hepatocellular carcinoma cells.* Oncotarget, 2015, 6(28): pp 25390–25401.

23. MacDonald B., Tamai K., He X. *Wnt/β-catenin signaling: components, mechanisms, and diseases.* Developmental Cell, 2009,17(1): pp 9-26.

24. Moro E., Vettori A., Porazzi P., Schiavone M., Rampazzo E., Casari A., Ek O., Facchinello N., Astone M., Zancan I., Milanetto M., Tiso N., Argenton F. *Generation and application of signaling pathway reporter lines in zebrafish.* Molecular Genetics and Genomics, 2013, 288(5): pp 231–242.

25. Pilichou K., Thiene G., Bauce B., Rigato I., Lazzarini E., Migliore F., Marra M. P., Rizzo S., Zorzi A., Daliento L., Corrado D., Basso C. *Arrhythmogenic cardiomyopathy.* Orphanet Journal of Rare Diseases, 2016, 11: pp 33.

26. Pinamonti B., Brun F., Mestroni l., Sinagra G. *Arrhythmogenic right ventricular cardiomyopathy: From genetics to diagnostic and therapeutic challenges.* World Journal of Cardiology (WJC), 2014, 6(12): pp 1234–1244.

27. Rampazzo A., Calore M., van Hengel J., van Roy F. *Intercalated Discs and Arrhythmogenic Cardiomyopathy.* Circulation: Cardiovascular genetics, 2014, 7: pp 930–940.

28. Rampazzo A., Nava A., Malacrida S., Beffagna G., Bauce B., Rossi V., Zimbello R., Simionati B., Basso C., Thiene G., Towbin J. A., Danieli G. A. *Mutation in human desmoplakin domain binding to plakoglobin causes a dominant form of arrhythmogenic right ventricular cardiomyopathy.* American Journal of Human Genetics, 2002, 71(5): pp 1200-6.

29. Rao F., Yuan Z., Zhang D., Yu F., Li M., Li D., Jiang B., Wen Y., Zhang P. Small-Molecule SB216763-Loaded Microspheres Repair Peripheral Nerve Injury in Small Gap Tubulization. Frontiers in Neuroscience, 2019, 13: pp 489.

30. Sen-Chowdry S., Lowe M. D., Sporton S. C., McKenna W. J. *Arrhythmogenic right ventricular cardiomyopathy: Clinical presentation, diagnosis, and management.* The American Journal of Medicine, 2004, 117(9): pp 685-95.

31. Sen-Chowdry S., Syrris P., Prasad S. K., Hughes S. E., Merrifield R., Ward D., Pennell D. J., McKenna W. J. *Left-Dominant Arrhythmogenic Cardiomyopathy: An Under-Recognized Clinical Entity. Journals of the American College of Cardiology, 2008, 52(25): pp 2175-87.*

32. *Smith L. L., Beggs A. H., Gupta V. A. Analysis of Skeletal Muscle Defects in Larval Zebrafish by Birefringence and Touch-evoke Escape Response Assays. Laura L. Smith, Alan H. Beggs, and Vandana A. Gupta.* Journal of Visualized Experiments (JOVE), 2013, (82):e50925.

33. Thiene G., Nava A., Corrado D., Rossi L., Pennelli N. *Right Ventricular Cardiomyopathy and Sudden Death in Young People*. The New England Journal of Medicine, 1988, 318(3): pp 129-33.

34. Yuan Z. Y., Cheng L. T., Wang Z. F., Wu Y. Q. *Desmoplakin and clinical manifestations of desmoplakin cardiomyopathy.* Chinese Medical Journal, 2021, 134(15): 1771–1779.

35. Zhurinsky J., Shtutman M., Ben-Ze'ev A. *Plakoglobin and b-catenin: protein interactions, regulation and biological roles.* Journal of Cell Science, 2000, 113(18): pp 3127-39.